A novel role for CRIM1 in the corneal response to UV and pterygium development

Eleonora Maurizi[1], Davide Schiroli[1], Sarah D. Atkinson[1,2], Laura Mairs[1], David G. Courtney[1], Barry O'Hagan[1], Victoria E. McGilligan[1,2], Alastair T. Pagnamenta[3], Jenny C. Taylor[3], Jesus J.D. Vasquez[4], Daniel E. Illanes-Velarde[4], Dave Goldsmith[5], Pieter Gouws[6], Jonathan E. Moore[1], M. Andrew Nesbit[1*], C.B. Tara Moore[1*].

Affiliations

[1] Biomedical Sciences Research Institute, Ulster University, Coleraine, Northern Ireland, BT52 1SA, UK.

[2] Northern Ireland Centre for Stratified Medicine, Biomedical Sciences Research Institute, C-TRIC Building, Altnagelvin Area Hospital, Ulster University, Derry/Londonderry, BT47 6SB, UK.

[3] Wellcome Trust Centre for Human Genetics, University of Oxford, Oxford, UK.

[4] Facultad de Medicina, Santa Cruz de la Sierra, Santa Cruz, Bolivia.

[5] Andean Medical Mission, 42, Sherwood Road, Bognor Regis, West Sussex, PO22 9DR, UK.

[6] Conquest Hospital, The Ridge, St Leonards-on-Sea, East Sussex, TN37 7RD, UK.

* To whom correspondence should be addressed: Biomedical Sciences Research Institute, University of Ulster, Coleraine, Northern Ireland BT52 1SA, United Kingdom. Tel no: +44(0)2870124577. Fax no: +44(0)28703324915. Email: a.nesbit@ulster.ac.uk, t.moore@ulster.ac.uk.

The authors wish it to be known that, in their opinion, the last two authors should be regarded as co-corresponding authors.

ABSTRACT

Pterygium is a pathological proliferative condition of the ocular surface, characterized by formation of a highly vascularized, fibrous tissue arising from the limbus that invades the central cornea leading to visual disturbance and, if untreated, blindness. Whilst chronic ultraviolet (UV) light exposure plays a major role in its pathogenesis, higher susceptibility to pterygium is observed in some families, suggesting a genetic component.

In this study, a Northern Irish family affected by pterygium but reporting little direct exposure to UV was identified carrying a missense variant in *CRIM1* NM_016441.2: c.1235 A>C (H412P) through whole-exome sequencing and subsequent analysis. *CRIM1* is expressed in the developing eye, adult cornea and conjunctiva, having a role in cell differentiation and migration but also in angiogenesis, all processes involved in pterygium formation. We demonstrate elevated *CRIM1* expression in pterygium tissue from additional individual Northern Irish patients compared to unaffected conjunctival controls.

UV irradiation of HCE-S cells resulted in an increase in ERK phosphorylation and *CRIM1* expression, the latter further elevated by the addition of the MEK1/2 inhibitor, U0126. Conversely, siRNA knockdown of *CRIM1* led to decreased UV-induced ERK phosphorylation and increased *BCL2* expression.

Transient expression of the mutant H412P *CRIM1* in corneal epithelial HCE-S cells showed that, unlike wild-type *CRIM1*, it was unable to reduce the cell proliferation, increased ERK phosphorylation and apoptosis induced through a decrease of *BCL2* expression levels.

We propose here a series of intracellular events where *CRIM1* regulation of the ERK pathway prevents UV-induced cell proliferation and may play an important role in the in the pathogenesis of pterygium.

Keywords: CRIM1; pterygium; UV; proliferation; ERK; apoptosis; variant

Abbreviations: BCL2, B-cell lymphoma 2; **BMP,** Bone Morphogenetic Proteins; **CRIM1**, Cysteine Rich Motoneuron protein1; **EMT,** Epithelial mesenchymal transition; **ERK (I)**, Extracellular signal–regulated kinases (Inhibitor); **HCE-S**, Human Corneal Epithelial cells; **IC,** Impression Cytology; **IGV,** Integrative Genomic Viewer; **MAF,** Minor allele frequency; **MAPK**, Mitogen-activated protein kinases; **MTT,** 3-(4,5-dimethylthiazol-2-yl)-2,5-diphenyltetrazolium bromide; **NGS,** Next Generation sequencing; **NI,** Northern Irish; **PolyPhen,** Polymorphism Phenotyping; **SIFT**, Sorting Intolerant From Tolerant**; TiGER,** Tissue-specific Gene Expression and Regulation; **TGF-β (I)**, Transforming Growth Factor- β (Induced); **TUNEL,** Terminal deoxynucleotidyl transferase dUTP nick end labelling; **VEGFA,** Vascular Endothelial Growth FactorA; **VW(F)-C,** Von Willebrand (Factor) C; **WES,** Whole Exome Sequencing.

1. INTRODUCTION

Pterygium (OMIM 178000) is a triangular shaped proliferative fibrovascular growth arising from the corneal-scleral limbus that invades the cornea centripetally[1,2]. The corneal invasion, through an active process of cell proliferation, matrix remodelling, angiogenesis and inflammation[1,3], results in astigmatism, irritation, tearing, and, if the visual axis is impinged upon, blindness in the most severe cases[4]. The only effective treatment for pterygium is surgical excision which, together with various adjuvant therapies, still presents a 12% recurrence rate[5]. A small conjunctival lesion, pinguecula, is considered to be related to pterygium with a similar aetiology[6], limbal localisation[7] and histology[8].

The main trigger for pterygium has long been attributed to UV radiation[9-11], with epidemiologic studies showing an average prevalence of 22% (as high as 40% in some Chinese populations[12] or 45% in provincial Indonesia[13]) in the "pterygium belt", an equatorial zone between latitudes 40°N and 40°S, compared to only 2% outside this area[4]. The human cornea represents a shield to protect the anterior eye from UV light and its anisotropic properties ensure that UV transmittance is reduced with a lower wavelength: while UVB (290-320nm) is completely absorbed by corneal epithelium, UVA (320-400nm) is absorbed only by 20% by the epithelial layer with the rest reaching the underlying stroma[14]. Focussing of incident light upon the nasal limbus has been proposed as the mechanism for the more frequent occurrence of pterygia at this location[15].

In pterygium, while UVB mediates oxidative DNA damage[16,17] and induction of cytokines and growth factors[18], both UVB[19] and UVA[20] are responsible for activation of ERK intracellular pathway.

Irritation and chronic inflammation caused by sand, dust and wind[21], as well as viral infections[22,23], have been suggested as additional environmental triggers for pterygium.

A genetic contribution to the incidence of pterygium was suggested in an Australian study[24], which revealed that 38% of patients admitted to hospital for excision of pterygia reported relatives

with the disease, and in studies where different ethnic groups living at the same geographical location display differing prevalence of pterygium[12,25].

High incidence of pterygium has been reported in a number of multigenerational families[26,27] and in monozygotic twins[28,29], where the most commonly reported mode of inheritance is autosomal dominant with reduced penetrance[4,30,31].

The lack of large families presenting with multiple affected individuals, compounded by the late-onset of the disease, together with incomplete penetrance, has hampered identification of causative genes for pterygium.

Candidate gene association studies, which derive from hypotheses in which the cause of pterygium is already assumed, have identified an increased predisposition to pterygium in individuals carrying germline mutations in genes related to: oxidative stress[16,32], carcinogenesis[33] or angiogenesis[34]; even though these analyses have been found subject to false-positive associations[35]. Next-generation sequencing techniques, such as Whole Exome Sequencing (WES) and Whole Genome Sequencing (WGS), provide a largely hypothesis-free approach to identifying causative genes in smaller families with fewer affected members[36].

In this study, using a WES approach, combined with bioinformatic and functional analysis, we identified a missense variant, p.His412Pro, in the *CRIM1* (cysteine rich motor neuron protein 1) gene, found in pterygium affected members of large multigenerational Northern Irish family with a documented small exposure to sunlight. *CRIM1* response to UV exposure revealed, for the first time, a central role within an intracellular mechanism involving ERK phosphorylation and ultimately leading to cellular proliferation or apoptosis. Introduction of the H412P variant in *CRIM1* resulted in an impairment of the whole pathway, demonstrating its possible involvement in the NI family's pterygium pathogenesis.

2. MATERIALS AND METHODS

2.1 Patient clinical examination

Clinical examinations were performed at Cathedral Eye Clinic, Belfast, UK (pterygium family members, pterygium and control individual samples from Northern Ireland).

A total of 24 patients from three consecutive generations of a Caucasian Northern Irish family affected by pterygium were investigated: three with pterygium, two with pinguecula and one unaffected family member participated to the WES study. Additional Northern Irish and Bolivian individuals (pterygium affected and unaffected controls) were recruited for sequence analysis of *CRIM1* and *CRIM1* expression analysis.

Following informed consent, collection of blood, tissues and a completed questionnaire was obtained from each participating individual under ethical approval from ORECNI Northern Ireland, UK (09/NIR01/14) and Comité de Bioética de la Facultad de Medicina, Santa Cruz, Bolivia.

2.2 Whole Exome Sequencing and Ingenuity Variant Analysis

WES was performed at the Wellcome Trust Centre for Human Genetics, University of Oxford. Briefly, genomic DNA was extracted from blood leukocytes using the QIAamp DNA Blood mini kit (QIAGEN, Manchester, UK), quantified by the high sensitivity Qubit system (Thermo Fisher Scientific, Loughborough, UK) and integrity of the DNA confirmed by electrophoresis on a 1% agarose gel.

The SureSelect Human All Exon v2 kit was used for Whole Exome capture according to the manufacturer's instructions (Agilent Technologies UK, Wokingham, Berkshire, UK). The SureSelect n.2100 Bioanalyser (Agilent Technologies) allowed an assessment of the quality of the exome enriched library obtained.

Parallel sequencing was then performed by Illumina GAIIx using 150bp-paired-end reads. Generated reads were aligned to the Human 37 reference genome with a short read mapper (Stampy) generating data in BAM format[37].

Coverage of the target region was verified to be in excess of 70% (greater than 10 reads). Platypus, an in-house variant caller able to detect Single Nucleotide Variants (SNVs) and short (<50bp) insertion/deletions (INDEL), was used to detect variant sites and alleles. Once the false positive rate was reduced, the resulting variants were stored as Variant Call Format (VCF) files. Ingenuity Variant analysis (Qiagen) was used to filter and select a smaller number of candidate genes. Aligned WES reads were viewed with the IGV platform. Clustal X2.1 was used to align CRIM1 sequences and results were visualized with EsPript 3.0 (http://espript.ibcp.fr)[38].

2.3 Sanger Sequencing

Sanger sequencing was performed on genomic DNA extracted from the blood leukocytes using QIAamp DNA Blood mini kit.

Presence of H412P in *CRIM1* was verified using the following primers: CRIM1_F: CTTCTTTTGCATGCACCCCC and CRIM1_R: TCACATGTGCAACCTTTCCTC while *CRIM1* VWFs were sequenced using genomic primers designed using Primer3[39] (Supplementary Table2). The PCR products were verified on a 1% agarose gel and Sanger sequenced at the Department of Zoology, University of Oxford.

2.4 Tissues and Impression cytology samples

Tissues samples (pterygium and normal cornea) were collected during surgeries while impression cytology samples were obtained using 4 x 4 mm strips of sterile LCR biopore membrane filter (pore size, 0.45 um; Millipore, Watford, UK) post pterygium surgery as previously described[40] and stored in RNAlater (Qiagen). Prior to IHC staining tissues were fixed in 95% ethanol for 20 minutes at room temperature. The RNA yield obtained from the impression cytology samples was never lower than 8ng/ul and never higher than 15ng/ul. The ratio of absorbance at 260 and 280

nm (A260/280) of the RNA samples was between 1.8 and 2.2. Samples for which the RNA yield was too low or the quality fell outside the limits were excluded.

2.5 Quantitative real-time PCR

RNA extracted using the RNeasy Plus Mini Kit (Qiagen, Manchester, UK) was quantified with the Nanodrop 1000 (Thermo Fisher Scientific) and 1 μg of total RNA was reverse transcribed into cDNA using the High Capacity cDNA Reverse Transcription Kit (Life Technologies, Paisley, UK). cDNA was used for qRT-PCR assays, performed using a Lightcycler 480 II (Roche, West Sussex UK).

Real Time Ready Assays for *CRIM1* (assay id. 112278), *VEGFA* (assay id. 140396), *SRCAP* (assay id. 126413), *TGF-βI* (assay id. 104720), Glyceraldehyde 3-phosphate dehydrogenase *(GAPDH)* (assay id. 141139) and hypoxanthine phosphoribosyltransferase *(HPRT*) (assay id. 102079) were purchased from Roche (Burgess Hill, West Sussex, UK).

SYBR green (Fermentas, Cambridge, UK) technology qRT-PCR was performed using *BCL2* primers (For AGCATGGGAGCCACGACCCT, Rev GGCCAAGGCCACACAGCCAA) and HPRT primers (For AGCTTGCGACCTTGACCAT, Rev GACCACTCAACAGGGGACAT), a kind gift from H. Nesbitt[41].

Data were normalised using *HPRT* and *GAPDH* as housekeeping controls for ΔCt and ΔΔCt calculations[42]. *HPRT* and *GAPDH* were chosen as they have been shown to be the most stable corneal housekeeping genes[43]. For each condition all complementary cDNA samples were run in duplicate in two independent experiments.

2.6 HCE-S culture

Human Corneal Epithelial cells (HCE-S), a spontaneously generated corneal cell line[44] (a kind gift from Prof. Julie Daniels), were cultured (37°C, 5% CO_2) in Dulbecco's modified Eagle's

medium (DMEM) containing 4 g/L glucose (Thermo Fisher Scientific, UK), and supplemented with 10% fetal bovine serum (Thermo Fisher Scientific, UK).

2.7 TUNEL assay

The terminal deoxynucleotidyl transferase dUTP nick end labelling (TUNEL) assay was performed on HCE-S cells which had been reverse transfected with Lipofectamine 2000 using a mock transfection with pGL4.17 [luc2/Neo] plasmid (Promega Madison, WI USA), *CRIM1* wild type or *CRIM1* H412P plasmids. After 72 hours cells were fixed with 4% paraformaldehyde (PFA) and stained using the In Situ Cell Death Detection kit (Fluorescein; Roche, Burgess Hill, Surrey, UK) following the manufacturer's instructions. Images were obtained using a fluorescent AxioScope A1 microscope equipped with an AxioCam MRc camera (Carl Zeiss, Germany); 10x objective. Twelve images for each condition (n=3) were quantified using ImageJ software (US National Institutes of Health) and then normalised to total DAPI cells in each field.

2.8 Immunohistochemistry (IHC)

Pterygium and conjunctival tissues were formalin fixed and paraffin embedded. Sections of 7μm were permeabilised with 0.5% Triton X-100 before staining, treated with Proteinase K solution (Fisher Bioreagents, BP1700-50, 10ug/ml in PBS) and blocked with 5% goat serum (Sigma). A rabbit polyclonal CRIM1 antibody (Abcam- ab189203) was incubated at 1:100, with a rabbit IgG (Abcam) used as an isotype control. Secondary antibody fluorescein isothiocyanate (FITC)-conjugated goat anti-rabbit IgG (Santa Cruz, USA) was used at a 1:100 dilution. Each section was mounted with fluorescent mounting medium (DAKO) and imaged using a 20× N Archoplan lens on an AxioScope.A1 microscope equipped with an AxioCam MRc camera (Carl Zeiss, Germany).

2.9 Site Directed Mutagenesis

Human CRIM1 cloned into a pcDNA3.1 plasmid was a kind gift from Dr. L Wilkinson, Institute for Molecular Bioscience, University of Queensland, Brisbane, Australia[45]. Site directed mutagenesis was performed to obtain the H412P *CRIM1* clone, using the Quick Change II kit

(Agilent Technologies), following the manufacturer's instructions. The entire *CRIM1* sequence was checked for integrity by Sanger Sequencing (Department of Zoology, University of Oxford), primers used are listed in Supplementary Table1.

2.10 MTT assay

Reverse transfection was performed in 12 well plates using HCE-S cells with either pCas9D10A_GFP (Addgene/Zhang lab), *CRIM1* wild-type or H412P plasmids with Lipofectamine 2000, according to the manufacturer's instructions (Falcon #353043, BD Corning Life Sciences, MA, USA). The following day cells were transferred in 96 well plates and 3-(4,5-dimethylthiazol-2-yl)-2,5-diphenyltetrazolium bromide (MTT) was added to the medium. Following 2 hours of incubation, the cells were resuspended in DMSO (Dimethyl sulfoxide, Sigma), absorbance was measured at 570 nm using the FLUOstar Omega (BMG Labtech, Aylesbury, UK) and quantified as relative percentages compared to control conditions. Absorbance measurements for the MTT were taken at 24, 48, 72 and 96 hours post transfection.

2.11 Western Blotting

HCE-S cells were cultured as described above. Low cell seeding densities were used to avoid cells becoming too confluent as this causes a decrease in ERK phosphorylation independent of the effect of CRIM1[46,47].

Proteins were extracted using Complete Lysis-M (Roche Diagnostics) and proteinase inhibitor (Sigma-Aldrich P8340), quantification of total protein was performed using the Bradford assay (BioRad), 25µg of the extracted proteins was then resolved on a 4-12% NuPAGE® Bis-Tris Precast Gels (Thermo Fisher Scientific UK) using NuPAGE® MOPS SDS Running Buffer and transferred onto Amersham TM Hybond ECL membrane (GE Healthcare Life Sciences).

Phospho ERK (#9101) and ERK (#9102) primary antibodies (Cell Signalling) were used at dilutions of 1:100 and 1:500 respectively with an overnight incubation at 4ºC. A secondary swine anti-rabbit antibody (DakoCytomation, Ely, UK) was used at a 1:2000 dilution for 1 hour at room

temperature. Protein binding was detected by standard chemiluminescence: SuperSignal™ West Pico Chemiluminescent Substrate (Thermo Fisher Scientific UK) and imaged using the G:BOX transilluminator (Syngene). Quantification was performed using GeneTools image analysis software: average peak values of phosphoERK were normalised against the average ERK values. All the results obtained were then normalised to the transfection control.

2.12 UV treatment and MEK1/2 inhibitor

HCE-S cells were seeded in a 24-well plate at 1×10^5 cells per well in growth medium and left to adhere overnight at 37ºC and 5% CO_2. The following day they were treated using a UVA cross-linker (IROC Innocross AG, Ramsen, Switzerland) delivering a dose of 5.4 J/cm^2 as previously described [48] or UVB at a final dose of 0.5 J/cm^2 through Arcadia D3 6% lamp (Arcadia, UK) with an aluminium reflector at a distance of 15 cm from the cells for 34 minutes.

The same doses of UVA and UVB irradiation were used in experiments in which the inhibitor of ERK phosphorylation (MEK1/2 inhibitor, U0126) was added to culture media an hour prior to the UV treatment as previously described[20], at a concentration of 10μM.

After irradiation, HCE-S cells were incubated in culture medium at 37°C with 5% CO_2 and harvested at 1, 6, 12, 24 and 48 hours.

2.13 siRNA transfection

Four different siRNAs targeting the *CRIM1* sequence (Set of 4 Upgrade: ON-TARGETplus CRIM1 siRNA, LU-008492-00-0002, 2nmol, Dharmacon) were reverse transfected in HCE-S cells using Lipofectamine RNAiMAX (Fisher Thermo Scientific), following the manufacturer's instructions. The four siRNAs were transfected singularly or as a pool at a final concentration of 10nM and normalised to the results from a non-specific siRNA control (NSC4) [49]. A range of different concentrations (0.2-0.5-1-10nM) of the siRNA pool reverse transfected in HCE-S cells was subsequently tested.

2.14 Statistical Analysis

All error bars represent the standard error of the mean (SEM) calculated between sample replicates of the same biological group. qRT-PCR, MTT and TUNEL assays significance was estimated using a Student's t-test calculation or the Mann-Whitney U test in GraphPad Prism 5 software with data illustrated using Box plots (qRT-PCR in Fig.3). p value ≤ 0.05 was deemed to be significant (*p value ≤ 0.05, **p value ≤ 0.01 and ***p value ≤ 0.001).

3. RESULTS

3.1 WES analysis in a Northern Irish family affected by pterygium and pinguecula

A multigenerational Northern Irish family presenting with pterygium and pinguecula, but not other eye abnormalities, was examined (Fig.1A). Pterygium affected both males and females and was diagnosed at an average age of 48 years. No history of unusual sun exposure was recorded for any family member, suggesting a familial predisposition for development of pterygium/pinguecula (Table 1).

Six members of this family underwent WES: three were affected by pterygium (II.2, II.4 and II.14, 72, 70 and 65 years old respectively), two by pinguecula (III.5 and III.6, 48 and 46 years old respectively), shown in Fig.2B, and one was unaffected (II.9, 58 years old). The other two younger unaffected members of the family (III.2 and III.3, age 49 and 34) did not participate in the WES but were subsequently analysed by Sanger Sequencing.

WES resulted in the identification of 451,153 variants in 18,858 different genes which were filtered in a stepwise manner by Variant analysis software (Ingenuity®) (Fig.1C). Selecting only those variants with a call quality ≥ 50 in any case and ≥ 20 in the control and a read depth ≥ 10; 30,000 variants were obtained. When variants with a minor allele frequency (MAF) greater than 0.5% (pterygium prevalence in Europe is 2%) in 1000 Genomes Project, ESP EA exomes and

Complete Genomics genome were excluded, the number of variants was reduced to 25,000. Analysis using either of the two algorithms Polyphen and SIFT, predicted as deleterious 11,000 variants, while 40 variants were finally selected as displaying an autosomal dominant segregation pattern within the family (Table 2).

Genes carrying mutations previously associated with pterygium such as *Ku70, GSTM1*, *ACE hOGG1*[16,17,33,34] were not observed in the selected list of variants.

Each single variant obtained by this analysis was then manually reviewed for determination of protein structure/function in Polyphen and SIFT, conservation of the amino acid among species running BLAST or eye expression interrogating Tiger Expression database. Literature was reviewed for any possible known correlation between gene mutations and pterygium or other diseases, either of the eye or otherwise. Moreover, adequate sequencing coverage and co-segregation of the variant within the family were verified through Integrative Genomic Viewer (IGV) (Table 2).

Based on the gene expression profile and on the known role in the eye, we selected *CRIM1* as our most plausible candidate gene. Recent studies have elucidated the importance of CRIM1 expression in corneal and conjunctival development[50-52] and the same variant, H412P, was identified from another WES study on patients affected by Coloboma eye developmental disorder[53]. Moreover, CRIM1 revealed a role in cell proliferation[54-56], adhesion and migration[57-59], angiogenesis through VEGFA[60-62] and UV-related diseases[63,64], the main processes involved in pterygium development[4].

3.2 CRIM1 structure and sequence analysis in individuals from Northern Ireland and Bolivia.

Presence of the variant in each affected family member, and absence from the unaffected sibling (II.9), was confirmed by direct Sanger sequencing (Fig.2A, example) of PCR products spanning the variant in VWFC-2.

Sequence alignment of *CRIM1* orthologues revealed residue H412 being conserved throughout human (*Homo sapiens*), cattle (*Bos Taurus*), mouse (*Mus musculus*), rat (*Rattus norvegicus*), frog (*Xenopous laevis*), zebrafish (*Danio rerio*) (Fig.2B).

CRIM1 is a 1002 amino acid transmembrane protein (once the 34 amino acid signal peptide has been cleaved) and consists of a large N-terminal extracellular portion composed of 11 domains (six Von Willebrand factor C, four antistasin-like and one Insulin-like Growth Factor-binding Protein (IGFBP)), a 21 amino acids transmembrane domain and a small 76 amino acid C-terminal cytoplasmic domain[65] (Fig.2C).

Although H412, located in the second VWFC domain, is not conserved in the other five VWFC of *CRIM1* (Fig.2D), it is conserved in the VWFC-2 domain of human chordin and in the VWFC-2 and 3 domains of human neuralin[66], two related bone morphogenic protein (BMP) antagonists, like CRIM1, all of which have a proven role during embryogenesis[45] (Fig.2E).

Sequence analysis of VWFC-2 in two additional younger family members (III.2 and III.3, age 49 and 34) revealed them to possess the same H412P variant; despite these individuals not having developed any signs of the disease. This is not incompatible with the mutation predisposing to the pathology, since a pattern of reduced penetrance has been widely described in familial pterygium[1,4,26].

All the CRIM1 VWFC domains are important for interaction with BMPs 4 and 7[45,67] as well as with VEGFA, TGF-β and PDGF: if any of those domains are deleted, the interaction with the TGF-β superfamily members is disrupted[62]. VEGFA, TGF-βs and PDGF have an important role in pterygium formation[3,68]: an altered interaction of those factors with CRIM1 VWFC domains could therefore have a role in pterygium development. Sanger sequencing analysis was subsequently performed for all the six VWFC domains of *CRIM1* (primers listed in Supplementary Table2) in genomic DNA obtained from two ethnically different populations: 12 affected individuals from Northern Ireland and 9 from Bolivia (Table3).

While the H412P variant was found in none of the pterygium affected individuals, one patient from Bolivia, B1 (Table3), presented with a cytosine to thymine transition in the first position of codon 745, predicted to result in an Arginine to Cysteine (R745C) amino acid change (dbSNP: rs145721446) between VWFC-4 and VWFC-5 (exon 13). Although the MAF of this variant is 0.000008237 (Supplementary Fig.1A) and the R745C variant is predicted to be possibly damaging by PolyPhen, this arginine residue is not conserved in other species and is substituted by histidine in cattle, mouse, and rat, and by serine in both frog and zebrafish (Supplementary Fig.1B). The significance of this sequence variant is unclear and not explored here.

3.3 CRIM1 expression analysis

Global expression databases indicated *CRIM1* expression in the whole eye, without differentiating between specific tissues. The location of CRIM1 expression in pterygium tissue and normal conjunctiva from sporadic Northern Irish individuals was therefore assessed by immunohistochemistry (IHC) and qRT-PCR (Fig.3).

CRIM1 was detected, by IHC, lengthwise across the whole pterygium tissue: from the anterior head (Fig.3A) to the posterior tail (Fig.3C). Moreover, CRIM1 was observed both in the external hypertrophic conjunctival epithelium and in the internal fibroblasts, in particular in the vascular endothelial cells surrounding the blood vessels (Fig.3C arrows).

Within the pterygium stroma, CRIM1 was found around unusual structures such as hair follicles and inside sebaceous glands (Fig.3B). Finally, CRIM1 was detected in normal conjunctiva (Fig.3E) and in post-surgical impression cytology samples of unaffected individuals (Fig.3F).

CRIM1 expression level was further investigated using qRT-PCR on RNA obtained from post-surgical impression cytology samples (Fig.3F) of unrelated Northern Irish (4 pterygium and 4 controls) individuals, together with a sample from a Northern Irish affected family member (II.2), found with the *CRIM1* H412P variant (Fig.3G).

CRIM1 expression is significantly higher in pterygium tissues when compared to unaffected conjunctival controls ($2^{-\Delta Ct}$ mean values are 4.22 ± 0.76 and 1.28 ± 0.122, while median values are 3.4 and 1.3 respectively, p = 0.028). Intriguingly, *CRIM1* expression in the Northern Irish family member II.2 pterygium is lower than that of the all unaffected controls from NI ($2^{-\Delta Ct}$ value of 0.32).

Thus, we have shown that CRIM1 expression, both at the RNA and protein level, is higher in pterygium than in unaffected control tissue.

3.4 Effects of UV on CRIM1 expression in corneal epithelial (HCE-S) cells

UV radiation is considered the main epidemiologic factor responsible for pterygium and pinguecula development[9-11]. Although some papers state that pterygium originates from conjunctiva and Tenon's fibroblasts[69], the common consensus is that the first trigger for pterygium development occurs at the limbal area[1,2,70-72] and pterygium growth has often been described as a localised limbal stem cell deficiency[70]. Since the aim of this paper is studying the early events triggering pterygium development, we considered that the best model would be a cell line coming from the zone where the initial events characterizing the disease have been described: the limbus. For this reason, for *in vitro* experiments we chose the HCE-S cell line, which spontaneously originated from corneal cells of the limbal area[44].

The effects of UV light exposure upon HCE-S cells *in vitro* were therefore investigated. The average daily dose of UV light has been estimated to be 60-70 J/cm^2 in central Europe[74]. Considering one hour exposure daily in general population, we irradiated an HCE-S monolayer to a dose of 5.4 J/cm^2 UVA[20,75], and a dose of 0.5 J/cm^2 UVB.

Following UVA exposure, *CRIM1* expression started increasing from 3 hours, becoming significantly different from untreated control by 6 hours and continuing up to 24 hours ($2^{-\Delta\Delta Ct}$ ± SEM values at 3, 6 and 24 hours are respectively: 0.90 ± 0.15, 8.59 ± 0.22 $p \leq 0.05$ and 10.39 ±

0.40 $p \leq 0.01$) (Fig.4A). UVB resulted in a significant increase in *CRIM1* expression at 24 hours after the treatment when compared to the untreated control ($2^{-\Delta\Delta Ct}$ ± SEM values at 3, 6 and 24 hours are respectively: 1.31 ± 0.03, 0.90 ± 0.01 and 1.95 ± 0.008, the last with a $p \leq 0.05$). Since irradiation with UVA has similar, but greater effects on *CRIM1* expression than UVB, subsequent experiments were conducted using UVA alone.

ERK phosphorylation, previously shown to be increased in pterygium cells following UVA exposure [19,20], was assessed in UVA-treated HCE-S cells as described above. This resulted in a 5.6-fold increase in ERK phosphorylation compared to the untreated control at 6 hours after UVA treatment, rising to 32.1-fold higher at 24 hours (Fig.4B). Treatment of HCE-S cells with the MEK1/2 inhibitor, U0126, prior to UVA irradiation resulted in a complete inhibition of UVA-induced ERK phosphorylation.

Since UVA significantly elevated both *CRIM1* expression and ERK phosphorylation at 24 hours after treatment, the effects of inhibition of ERK phosphorylation on *CRIM1* expression following UV irradiation were studied. Surprisingly, inhibition of ERK phosphorylation in HCE-S cells significantly ($p<0.001$) potentiated the UV-induced increase in *CRIM1* expression at 24 hours (UVA + inhibitor: 3.75 ± 0.12, UVA only: 1.82 ± 0.15, inhibitor only 0.77 ± 0.02, untreated control: 0.63 ± 0.07; values expressed as $2^{-\Delta Ct}$) (Fig.4C).

Several studies have shown that increased ERK activity is associated with a decreased expression of the anti-apoptotic transcription factor, B*CL2* and an increased apoptosis[76]. Increased expression of *BCL2* and decreased expression of apoptosis markers has been observed in pterygia[1,77]. With this in mind, the expression level of *BCL2* was investigated following UVA treatment activating the ERK pathway in HCE-S cells.

Either UVA treatment or inhibition of ERK phosphorylation in HCE-S cells alone significantly decreased *BCL2* expression ($2^{-\Delta\Delta Ct}$ ± SEM values for ERK-I: 0.53 ± 0.05 and UVA 0.48 ± 0.06; both $p \leq 0.05$) (Fig.4D). In comparison to those, when HCE-S cells were treated with MEK1/2

inhibitor, U0126, and UVA irradiation, *BCL2* expression was significantly increased ($2^{-\Delta\Delta Ct}$ ± SEM of 1.45 ± 0.13; $p \leq 0.001$) and restored levels seen in untreated cells ($p = 0.06$).

UV irradiation has therefore a fundamental role in triggering a series of events, including the increase of *CRIM1* expression and the phosphorylation of ERK, corresponding to a decrease in *BCL2* levels in HCE-S cells.

3.5 CRIM1 intracellular pathway triggered by UVA

CRIM1, ERK and BCL2, as shown above, are interrelated in playing a pivotal role in the intracellular pathway triggered by UV exposure in HCE-S.

To further investigate the relationship between those factors, we sought to assess the effects of knocking down expression of *CRIM1* following siRNA transfection. Four siRNAs targeting *CRIM1*, both separately and in a pool, efficiently knocked down endogenous *CRIM1* expression in HCE-S cells to less than 30% of untreated level, 48 hours after transfection ($p \leq 0.001$) (Supplementary Fig.2).

Endogenous levels of *CRIM1* expression in HCE-S, normalised to cells transfected with NSC siRNA, increased after UVA treatment by 1.7 ± 0.05 fold, $p \leq 0.05$. Because levels of *CRIM1* expression appear critical and finely regulated following UV irradiation, the concentration of siCRIM1 was titrated (0.2nM, 0.5nM, 1nm and 10nM) to establish the concentration at which *CRIM1* expression was the same as non-UVA treated, NSC4-tranfected HCE-S cells (Supplementary Fig.3). The siCRIM1 concentration at which this was achieved was 0.5nM (Fig.5A).

Since pterygium is considered a proliferative rather than degenerative condition[4,70] and UV light alters cell proliferation at the limbal area as the first event promoting pterygium formation[78], an MTT proliferation assay was then performed on HCE-S cells after UVA treatment (Fig.5B). UVA significantly increased HCE-S proliferation at 72 hours (Δabsorbance at 72-24 hours, control

0.53 ± 0.02 OD vs UVA 0.6 ± 0.03 OD; $p \leq 0.05$). When cells were transfected with 0.5nM siCRIM1 prior to UVA treatment, HCE-S proliferation was further increased relative to UVA treatment alone (Δabsorbance at 72-24 hours: 0.7 ± 0.02 OD, with $p \leq 0.05$ compared to UVA and $p \leq 0.01$ compared to the mock NSC4 control).

As previously shown (Fig.4B), ERK phosphorylation was significantly increased 24 hours after UV exposure. Transfection of cells with 0.5nM siCRIM1 prior to UV exposure almost completely abolished the increase in ERK phosphorylation (Fig.5C).

Finally, ERK and *CRIM1* regulation were related to *BCL2* expression levels (Fig.5D), which decreased significantly 24 hours after UVA treatment of HCE-S cells when compared with the untreated control ($2^{-\Delta\Delta Ct}$ values for UVA treated HCE-S: 0.61 ± 0.06, $p \leq 0.01$). However, prior transfection with 0.5nM siCRIM1 prevented the decrease in *BCL2* expression, and was not significantly different from mock NSC4 transfected cells ($2^{-\Delta\Delta Ct}$ values of siCRIM1+UVA: 0.96 ± 0.08).

The latest results obtained using siCRIM1 were able not only to confirm the previous data showing a UVA-mediated increase in *CRIM1* expression, ERK phosphorylation and a decrease in *BCL2* expression, but also to demonstrate that by modulating only *CRIM1* expression, the whole signalling pathway leading to cell proliferation in response to UVA exposure can be regulated.

3.6 Effects of wild type and H412P mutant CRIM1 over-expression in HCE-S cells

Based on the outlined pathway involving CRIM1 regulation upon UV exposed HCE-S cells, the consequences of the H412P *CRIM1* variant in a pterygium pathogenic context were investigated. The H412P variant was introduced into the human *CRIM1* sequence by site directed mutagenesis and the complete *CRIM1* sequence checked by Sanger sequencing (Supplementary Table1),

454 confirming the presence of the c.1235 A>C substitution and absence of any other variation in the
455 sequence.
456 HCE-S cells were transfected with an empty plasmid, wild type or the *CRIM1*:p.H412P
457 expression plasmid. A significant *CRIM1* overexpression with respect to endogenous *CRIM1* was
458 revealed by qRT-PCR both at 48 hours (*CRIM1* wt 6 ± 0.82, $p<0.01$ and *CRIM1* H412P 5.8 ±
459 0.97, $p<0.05$) and at 72 hours (*CRIM1* wt 6.4 ± 1.075, $p<0.01$ and *CRIM1* H412P 6.3 ± 1.4
460 $p<0.01$) after transfection (Fig.6A).
461 Since a decrease in proliferation was reported in vascular endothelial cells after transient CRIM1
462 overexpression[54], an *in vitro* MTT proliferation assay was then performed in HCE-S cells
463 transfected with *CRIM1* wild type or H412P constructs (Fig.6B). Compared to mock transfected
464 HCE-S cells, wild type *CRIM1* overexpression had a relevant anti-proliferative effect, which was
465 most significant at 72 hours post-transfection (Δabsorbance 72-24 hours 0.60 ± 0.02 OD; $p<0.01$).
466 This effect was not observed in the *CRIM1* H412P transfected cells (Δabsorbance 72-24 hours
467 0.52 ± 0.02 OD), which did not differ significantly from the mock transfected control
468 (Δabsorbance 72-24 hours 0.57 ± 0.01 OD).
469 ERK phosphorylation is increased, simultaneously with CRIM1 expression, in vascular
470 endothelial cells after VEGFA treatment[79]. Here, ERK phosphorylation was strongly increased in
471 the wild type *CRIM1* transfected HCE-S compared to mock transfected control and to H412P
472 *CRIM1* transfected cells at 72 hours post-transfection (Fig.6C).
473 Other gene expression levels, possibly affected by *CRIM1* H412P variant, were investigated
474 by qRT-PCR: *VEGFA* for its role in pterygium angiogenesis[3,72] and its direct interaction with
475 *CRIM1*[73], Transforming Growth Factor beta I (*TGF-βI*) for its involvement in several other eye
476 diseases[80] and *BCL2* for its importance in apoptosis, previously documented in pterygium[77,81].
477 HCE-S cells were transfected with wild type and H412P *CRIM1* plasmids and gene expression
478 was assessed at 48 and 72 hours after transfection (Fig.6D). Levels of *VEGFA* and *TGF-βI*

expression were not significantly different between the wild type and the H412P *CRIM1* transfected cells (*VEGFA*: wild type 48 hours 0.8351 ± 0.0740, H412P 48 hours 0.8966 ± 0.0630, wild type 72 hours 1.1447 ± 0.0940, H412P 72 h 1.0443 ± 0.1100, *TGF-βI*: wild type 48h 0.7410 ± 0.0730, H412P 48h 0.8630 ± 0.0480, wild type 72h 0.9428 ± 0.0650, H412P 72h 1.1810 ± 0.1080, all values are expressed in $2^{-\Delta Ct}$). In contrast, a significant decrease in *BCL2* expression level was observed in the wild type *CRIM1* transfected cells with respect to H412P mutant and mock transfected cells (p value <0.05) both at 48 and 72 hours (wild type 48 hours: 0.5453 ± 0.0720, H412P 48 hours: 1.1647 ± 0.1800 and wild type 72 hours: 0.5977 ± 0.0240, H412P 72 hours: 1.2376 ± 0.1350, all values are expressed in $2^{-\Delta Ct}$), suggesting that overexpression of *CRIM1* may play a role in up-regulation of apoptosis, which is normally induced in cornea and conjunctiva by UV radiation[82,83].

The effect of increased *CRIM1* expression upon apoptosis in HCE-S cells was investigated in *CRIM1* transfected cells by TUNEL assay (Fig.6E). At 72 hours after transfection the wild type *CRIM1* transfected HCE-S cells showed a significantly higher rate of apoptosis compared to either the H412P *CRIM1* or mock transfected HCE-S. The percentage of apoptotic (TUNEL positive), wild type *CRIM1* transfected cells (25.6 ± 1.8) was significantly higher than either H412P *CRIM1* plasmid or mock transfected HCE-S cells (3.9 ± 0.4 and 2.7 ± 0.5 respectively; p<0.001) (Fig.6E). We have shown here that *CRIM1* plasmid overexpression exerts the same effects of UV induced *CRIM1* increased intracellular levels, in terms of decreased cell proliferation, increase in ERK phosphorylation and reduction in *BCL2* expression, followed by a higher rate of apoptosis.

The presence of H412P variant in *CRIM1* however abolished any of those effects, supporting a role for this variant in the increased susceptibility of members of the Northern Irish family to pterygium and pinguecula.

4. DISCUSSION

UV light presents a chronic stimulus to the eye surface, altering the normal processes of growth control in cornea and conjunctiva, and is associated with several pathologies affecting the anterior eye[84] such as photokeratitis[85], climatic droplet keratopathy[10], cortical cataract[86], squamous cell carcinoma[87] and pterygium[9,21]. Pterygium, resulting in 1% of all the ocular surgeries in developed countries[88] and presenting a 12% surgery recurrence rate[5], represents a substantial cost to National Health Services and the community, estimated in Australia as US $100M per year[89]. In the identified Northern Irish family (Fig.1), affected by pterygium or pinguecula despite not being exposed to high levels of sunlight, genetic predisposition may play a fundamental role in the etiologic process (Table 1). A WES approach to candidate gene identification with *in silico* and literature analysis led to selection of H412P variant in *CRIM1* gene for several reasons. Firstly, the substitution of a highly conserved, positively charged histidine (H) residue with an apolar proline (P) is predicted to interfere with CRIM1 structure and function.

Moreover, the interaction between F1 domains of fibronectin, structurally similar to VWF domains of CRIM1 where H412P is located, and VEGF is enhanced at acidic pH (5.5-7)[66]. As Histidine works at this pH range (pKa_3=6), a mutation in this residue may interfere with the electrostatic binding of other ligands.

CRIM1's VWF domains (Fig.2) were also shown essential for interaction with VEGFA[62], the angiogenic factor overexpressed in the vascularised pterygium tissue following UV exposure[3,72]. CRIM1 is thus proposed as a VEGFA antagonist[60,73], possibly resisting pterygium formation by preventing angiogenesis as it has been shown to prevent proliferation[54,55]. Proliferation in cardiomyocytes is reduced by CRIM1 upregulation following miR199a silencing[55,56], the same miRNA which was found overexpressed in pterygium[90]. In addition to proliferation and angiogenesis, tissue remodelling through cell adhesion and migration also occurs during pterygium formation[4]. This process has been shown to be regulated by CRIM1 in neurons[57], lung

cancer[59] and lens epithelial cells[58], the latter showing a premature fibre differentiation when *CRIM1* is lost[91].

As previously described, pterygium etiopathogenesis is generally ascribed to UV eye exposure and *CRIM1* was found to be involved in UV related diseases such as bovine eye cancer[63] and melanoma[64]. Finally, recent studies have elucidated the importance of *CRIM1* expression during the anterior eye development[50,51,58].

CRIM1 was thus selected as our best candidate responsible for pterygium pathogenesis within the NI family. However, a reduced penetrance, as previously described in pterygium[1,26,31], makes interpretation of genetic data challenging[36]. While two unaffected members of the NI family (III.2 and III.3) harbour the H412P variant in *CRIM*1, no affected member was found that did not have the H412P variant. Moreover, given the younger age of the unaffected members (34 and 48 years old), penetrance in this case could be age-related, as described in MEN1 syndrome, in which tumour occurrence increases with the age, becoming fully penetrant only after sixty years[92]. It is therefore possible that III.2 and III.3 family members may never develop pterygium or will do so later in their lifetime; in any case, they should be monitored closely for development of pterygium in the future.

Neither the *CRIM1* H412P variant nor any other alteration within the six VWFC domains of *CRIM1* were found in other affected unrelated individuals from Northern Ireland.

Only one other patient from Bolivia was identified with a missense variant located between VWFC-4 and VWFC-5: R745C (Supplementary Fig.1). While this arginine residue is not conserved between the species, the introduction of a cysteine residue may facilitate disulphide bridge formation with highly conserved cysteine residues in the previous or subsequent VWFC domain, vital to the VWF domain's structure[45,93].

While no variants in *CRIM1* were found in the NI patients, CRIM1 expression was elevated throughout the pterygium tissue compared to unaffected conjunctiva (Fig.3). In particular, *CRIM1* expression was observed around pterygium blood vessels which, together with its previously

554 described expression in endothelial cells during capillary formation[60,61] and its interaction with
555 VEGFA[73], suggests a role for CRIM1 during the critical angiogenic processes of pterygium
556 formation[1,21]. CRIM1 was also detected in unusual structures such as hair follicles and sebaceous
557 glands, previously identified as characteristic features of some pterygia[70]. These structures are
558 representative of an uncontrolled transdifferentiation program[94] occurring in pterygium in
559 addition to an epithelial-mesenchymal transition (EMT) or fibrosis process[95], and likely reflects
560 similarities between pterygia, limbal dermoids and hair epithelia[96].
561 Comparing *CRIM1* expression levels between pterygium-affected and -unaffected individuals,
562 those were significantly increased in the affected samples (Fig.3G), while the lowest *CRIM1*
563 expression was recorded for the affected family member (II.2). A high *CRIM1* expression in
564 pterygium-affected individuals could therefore represent a defensive cellular response mechanism
565 against UV damaging effects, which is impaired by the H412P variant within the NI family.
566
567 Involvement of CRIM1 in UV-related diseases either in the eye[63] or the skin[64] is not surprising
568 considering that UV irradiation affects the balance between proliferation and apoptosis in several
569 cell types, including skin keratinocyes[97,98], corneal epithelium[82] and pterygium basal epithelial
570 cells[77]. However, while the eye is exposed to both UVA and UVB radiation, the intensity of UVA
571 radiation reaching the Earth's surface has 10-100 times the intensity of UVB[99] and it is known to
572 induce oxidative stress in exposed cells and tissues, including pterygium[100]. Accordingly, UVA
573 induced a more rapid and larger response than UVB in HCE-S cells (Fig.4A).
574 Exposure of HCE-S cells to UVA radiation leads to an increase in *CRIM1* (Fig.4A) expression.
575 The elevated ERK phosphorylation upon UVA irradiation we observed (Fig.4B) was previously
576 described in UVA or UVB irradiated pterygium and conjunctival cells[19,20]. While inhibition of
577 ERK phosphorylation alone had no effect on the expression of *CRIM1*, it potentiated the *CRIM1*
578 up-regulation when HCE-S cells were treated with UV (Fig.4C). This underscores the importance
579 of UV irradiation as the primary trigger for the intracellular pathway but underlines also the

capacity of ERK phosphorylation to regulate *CRIM1* expression levels. Moreover, inhibition of ERK phosphorylation in HCE-S cells treated with UV abolished the UV-induced decrease in *BCL2* expression (Fig.4D): UV decreases *BCL2* levels through ERK phosphorylation, which results therefore in upstream *BCL2* regulation within this pathway.

The role of CRIM1 in the cellular response to UV exposure was confirmed in HCE-S cells in which *CRIM1* over-expression induced by UV treatment was inhibited by siRNA transfection (Fig.5A). An increased cell proliferation in siCRIM1-treated cells upon UV exposure (Fig.5B), suggests that CRIM1 has a role in protecting against pterygium formation by minimising cell proliferation in response to UV radiation. When siCRIM1 was added to UV treatment, HCE-S cells decreased ERK phosphorylation to that seen in untreated cells (Fig.5C) and restored *BCL2* basal expression (Fig.5D), revealing that also *CRIM1* is able to control ERK phosphorylation as well as *BCL2* expression and locates it upstream of those two factors within the pathway. Those experiments showed how CRIM1 exerts a central role within the UV triggered intracellular pathway and silencing its expression is enough to counter all those alterations we examined.

Previous studies have shown how *CRIM1* alterations influences cellular function: multiple exon deletions of *CRIM1* lead to syndromic disease[52] while a minor alternately spliced *Crim1* isoform determines perinatal lethality with multiple organ dysfunction[51]; however, the effects of *CRIM1* missense mutations still remain unexplored. Therefore, based on the intracellular mechanism described, the effects of the H412P variant found within the Northern Irish kindred were studied. *CRIM1* over-expression in HCE-S cells leads to reduced proliferation (Fig.6B) and a parallel increase in apoptosis (Fig.6D), as expected following the previous results where *CRIM1* was shown having a protective role in pterygium formation, counteracting the UV-induced proliferation (Fig.4B). This is in accordance with the downregulation of vascular endothelial cell proliferation after transient *CRIM1* overexpression[54] and with the increase in cardiomyocyte proliferation following *CRIM1* silencing through miR-199a[55,56]. Since the same miR-199a was found upregulated in pterygium[90], this could analogously increase cell proliferation in pterygium

formation through *CRIM1* silencing, counteracting the protective effects of *CRIM1* overexpression.

CRIM1 overexpression was also able to increase ERK phosphorylation (Fig.6B) following UVA irradiation (Fig.4B). This result confirms previous data (Fig.5C) showing that the effects of *CRIM1* overexpression lie upstream of ERK phosphorylation and demonstrates that it does not need UV to exert its function.

All the effects of *CRIM1* overexpression in HCE-S cells were almost completely abolished by the H412P variant in *CRIM1* (Fig.6).

The results obtained delineated a finely regulated pathway where either UV (Figure 4B) or elevated CRIM1 levels (Figure 6C) increase ERK phosphorylation, demonstrating that CRIM1 lies upstream of, and is responsible for ERK phosphorylation.

CRIM1 expression was increased upon UV exposure and this increase was potentiated when the U0126 inhibitor was added to the UV-irradiated cells. This suggests a feedback mechanism in which ERK phosphorylation, increased by elevated *CRIM1* levels, serves to limit the rise in *CRIM1* expression triggered by UV (Fig.7). UV is therefore necessary for the activation of the whole pathway because the U0126 inhibitor alone, without UV treatment, does not increase CRIM1 expression (Figure 4C). For the first time an increase in *CRIM1* expression has been directly correlated with a consequent activation of the ERK pathway in corneal cells.

Based on the *in vitro* experimental evidence and on the feedback mechanism outlined, H412P can be considered either a loss-of-function or a dominant-negative mutation. Similarly, a study on a shortened mouse *Crim1* isoform was unable to conclude whether the mechanism was hypomorphic (reduced activity) or dominant negative[51], although the latter have been described in growth factor receptors which bind the same CRIM1 interactors such as PDGF[101] or VEGF[102] and in VWF domains similar to those found in CRIM1[103,104].

5. CONCLUSIONS

In summary, we have shown that *CRIM1* plays an important role in the response of corneal cells to UV irradiation by activation of a finely regulated intracellular pathway where increased *CRIM1* expression counteracts cell proliferation and increases apoptosis. We demonstrate that *CRIM1* H412P variant impairs this response, suggesting its involvement in the increased susceptibility to pterygium observed in a Northern Irish family. Further investigation of the role of CRIM1 in UV triggered pathways and pterygium holds promise as a target for the prevention and treatment of development or recurrence of pterygium or other UV related diseases.

6. ACKNOWLEDGEMENTS

The authors would like to thank the patients who were involved in this study and their invaluable contributions to this research.

The WES investigation was supported by the NIHR Biomedical Research Centre, Oxford.

Conflict of Interest Statement None declared.

Funding: Ulster University Vice-Chancellor's Research Scholarships (VCRS)

7. FIGURE LEGENDS

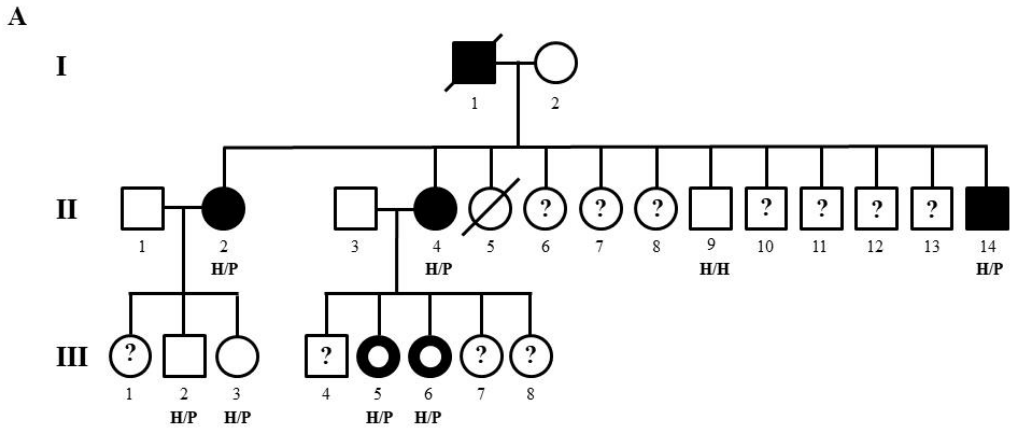

B

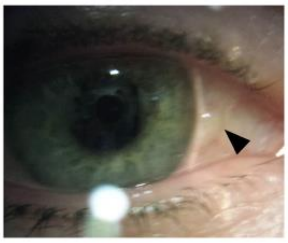

C

Filters	No. of variants
WES	451,153
Ingenuity Confidence	30,000
Ingenuity Common Variants	25,000
Ingenuity Predicted Deleterious	11,000
Ingenuity Genetic Screening	40
In silico, literature	1

Figure 1. Northern Irish family affected by pterygium or pinguecula and WES analysis. **(A).** Pedigree of a Northern Irish family affected with pterygium. Open symbols denote unaffected individuals; filled black symbols denote pterygium affected individuals and filled black symbols with open circles inside denote pinguecula affected individuals. Squares represent male and circles represent female individuals. Slashed symbols denote deceased family members and question marks are for individuals who have not participated in the study. Although all family members were invited to participate in this study, only those who gave informed consent were enrolled. **(B).** Pinguecula visible at the limbal area, between the cornea and conjunctiva (arrowhead). The image was obtained from family member III:5. **(C).** WES variants screening. Ingenuity variant analysis screened the 451,153 variants obtained with WES using four subsequent filters: Confidence to ensure quality, Common Variants (MAF < 0.05), Predicted deleterious using Polyphen and SIFT and Genetic, assuming an autosomal dominant inheritance pattern. A final *In silico* analysis based on the residue conservation through BLAST and Clustal Omega, expression analysis using TiGER database and literature research allowed selection of a single candidate variant in *CRIM1* gene.

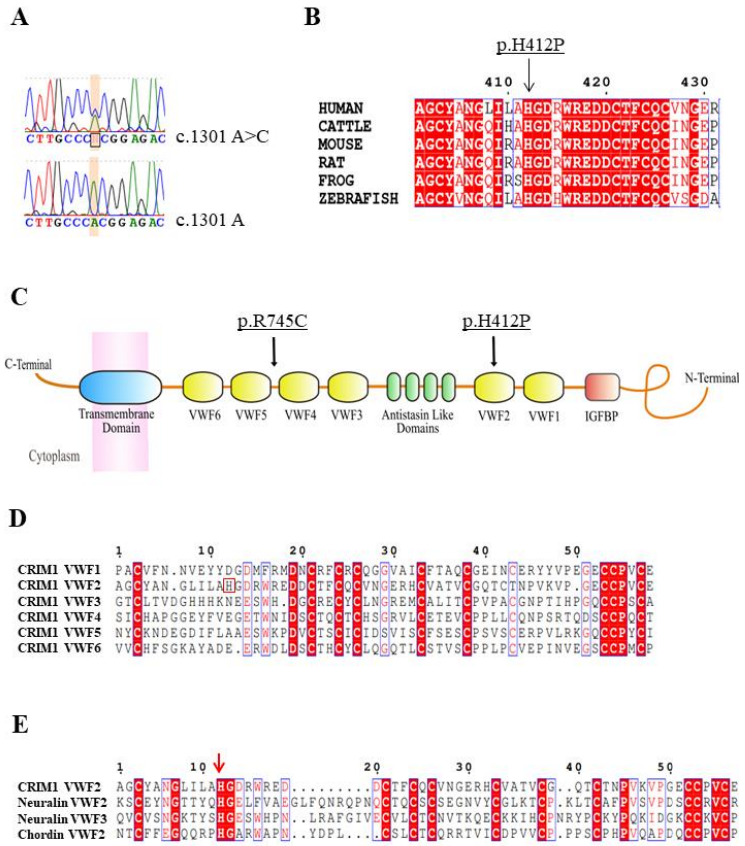

Figure 2. CRIM1 (Cysteine RIch transMembrane BMP regulator 1) sequence in the NI family, conservation and structure analysis. **(A).** Electropherogram of Sanger sequencing performed in the family members confirmed the c.1235 A>C heterozygous transversion mutation in affected individuals and which was homozygous for wild-type A allele in the unaffected control. **(B).** Clustal X2.1 multiple sequence alignment of orthologous CRIM1 protein sequences from Human (NP_057525.1), Cattle (NP_001192227.1), Mouse (NP_056615.1), Rat (NP_001162574.1), Frog (NP_001163917.1), Zebrafish (NP_997986.1) indicates that the H412P missense mutation occurs in a highly conserved residue. EsPript 3.0. Legend: Red box, white character: strict identity; Red character: similarity in a group; Blue frame: Similarity **(C).** Schematic ideogram of Human CRIM1, characterised by multiple domains: one transmembrane (blue), six von Willebrand factor (VWF) (yellow), four antistasin-like (green) and one IGFBP (red). The position of the H412P and the R745C mutation are indicated. **(D).** Clustal X2.1 alignment of the six VWFC domains in *CRIM1* shows that, other than in VWFC-2, H412 is not conserved in the other five VWFC domains. **(E).** Clustal X2.1

680 alignment of CRIM1 with other BMP antagonists indicates that the residue H412 is conserved in the
681 VWFC-2 domain of human chordin and in the VWFC-2 and 3 domains of human neuralin.
682 across groups (if more than 70% of the residues within the frame share similar physico-chemical
683 properties).
684

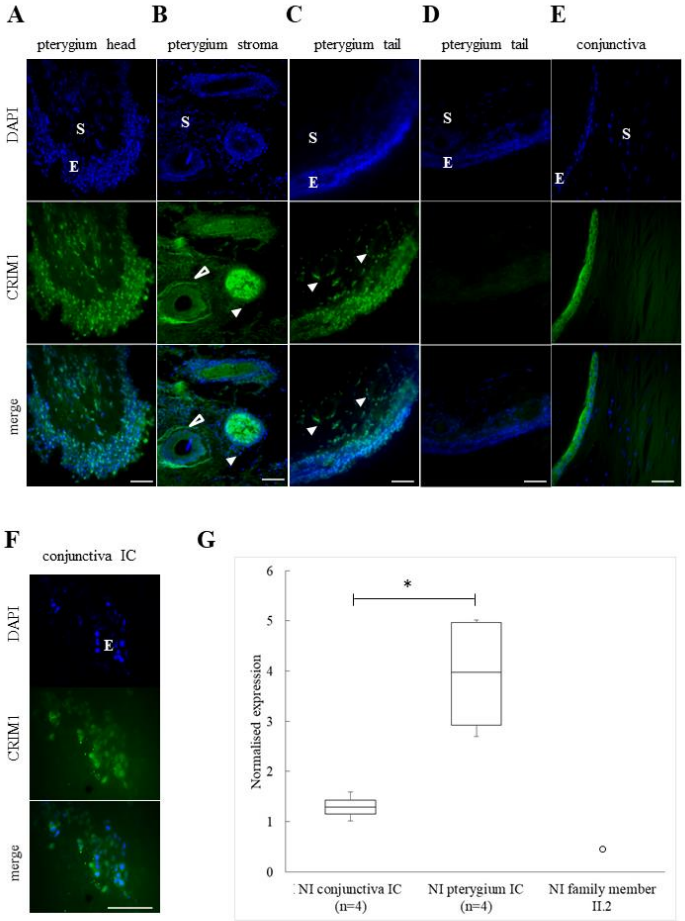

685

686 **Figure 3.** CRIM1 expression analysis in pterygium and conjunctiva from Northern Ireland. **A-F**
687 images represent immunohistochemical (IHC) staining of CRIM1 expression (green) and nuclei
688 (DAPI, blue) in pterygium and conjunctival tissues obtained from sporadic Northern Irish patients.
689 Scale bar, 100μm **(A).** CRIM1 expression in a pterygium head, visible in both the external epithelial
690 layer (E) as well as the internal stroma (S). **(B)**. CRIM1 expression shown in peculiar structures
691 identified in pterygium stroma: a hair follicle (empty arrowhead) and a sebaceous gland (plain
692 arrowhead). **(C).** CRIM1 expression in pterygium tail, arrowheads indicate CRIM1 expression in
693 cells surrounding the blood vessels. **(D).** Negative IgG control in pterygium tail tissue. **(E).** CRIM1
694 expression in conjunctival epithelial tissue of an unaffected individual. **(F).** IHC of a post-surgical
695 impression cytology sample obtained from unaffected superficial epithelial conjunctival cells:
696 CRIM1 is expressed in all the cells captured on the membrane filter. **(G)** *CRIM1* expression is

increased in pterygium patients from Northern Ireland. qRT-PCR analysis of *CRIM1* carried out in cDNA from post-surgical impression cytology samples: NI conjunctival individual controls, NI pterygium individuals and one affected NI family member (II.2 in Fig. 1). All values are expressed in $2^{-\Delta Ct} \pm$ SEM. n=2 with two technical replicates each sample.

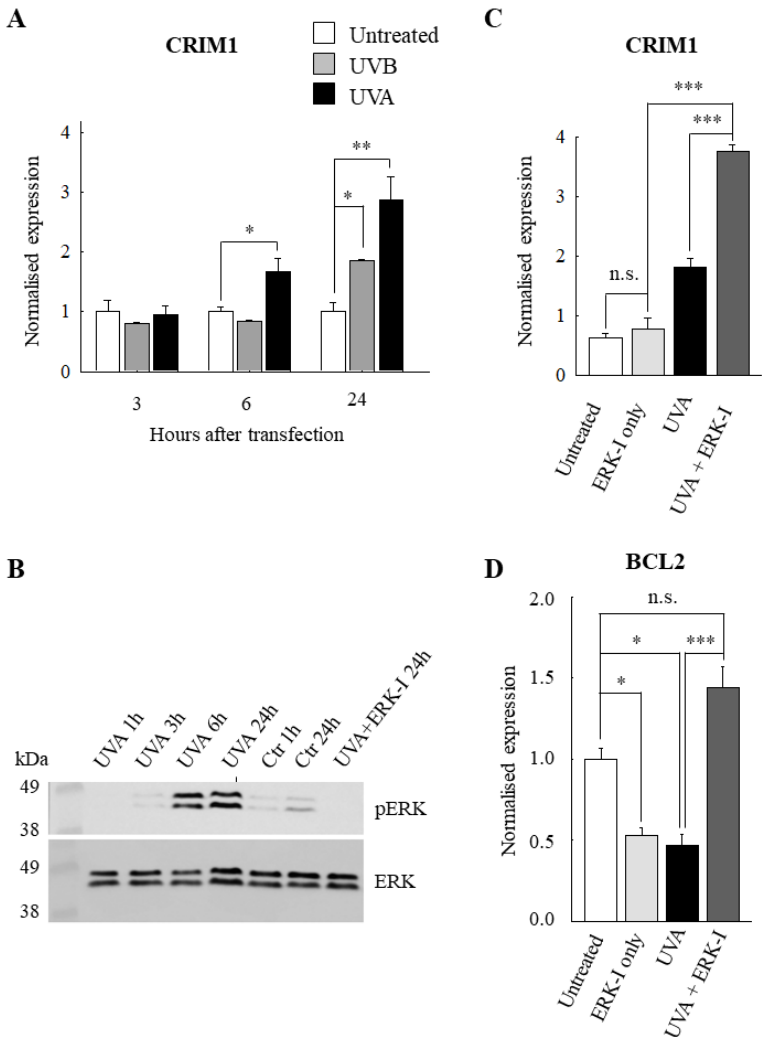

Figure 4. UV treatment of HCE-S cells increases CRIM1 expression, ERK phosphorylation and decreases BCL2 expression. **(A).** qRT-PCR revealed significantly increased CRIM1 expression levels in HCE-S cells at 6 ($p \leq 0.05$) and 24 hours ($p \leq 0.01$) after UVA treatment and at 24 hours ($p \leq 0.05$) after UVB treatment compared to the untreated control. **(B).** Western blot analysis of HCE-S cell lysates revealed an increase in ERK phosphorylation at 6 and 24 hours after UVA irradiation with respect to ERK phosphorylation levels of untreated control. Pretreatment of cells with U0126 inhibitor abolished ERK phosphorylation in UV treated cells. **(C).** qRT-PCR was used to evaluate *CRIM1* expression following UV treatment in the presence of MEK1/2 inhibitor, U0126. Inhibition of ERK pathway activation enhances the increase in *CRIM1* expression seen in UV irradiated HCE-S cells whilst inhibition of ERK phosphorylation alone has no significant effect. **(D).** *BCL2* expression measured by qRT-PCR. HCE-S cells were UVA irradiated with and without U0126 and

harvested 24 hours after treatment. A significant decrease in *BCL2* expression was observed when the cells were treated with either U0126 or UVA alone but not in combination when compared to the HCE-S untreated cells. qRT-PCR data represent fold change of the $2^{-\Delta\Delta Ct}$ mean ± SEM compared to untreated HCE-S. n=3 with three technical replicates each.

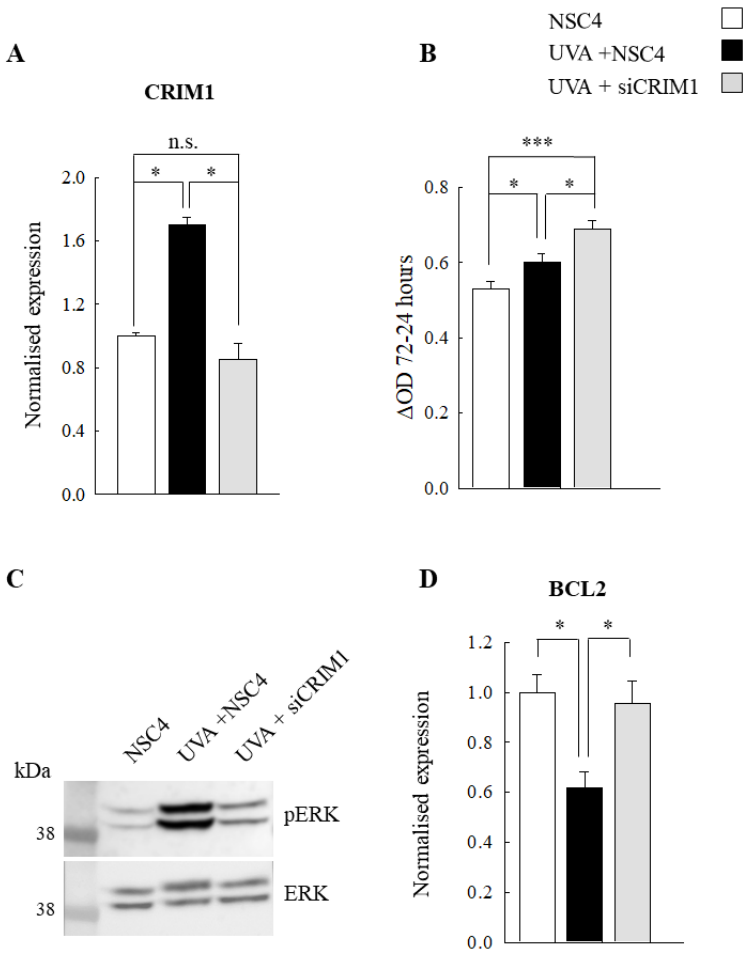

719

720 **Figure 5.** siCRIM1 0.5nM is able to restore normal HCE-S conditions after UVA treatment. **(A).**
721 qRT-PCR shows the amount of siCRIM1 (0.5nM) able to restore endogenous CRIM1 levels in
722 HCE-S after UVA exposure. For all the experiments HCE-S cells were treated with: NSC4, UVA +
723 NSC4 and UVA+ siCRIM1 (0.5nM) and harvested 24 hours later. Data represent $2^{-\Delta Ct}$ ± SEM. n=3
724 with three technical replicates for each sample. **(B).** An MTT assay demonstrates an increased
725 proliferation upon UVA exposure, which is further increased if *CRIM1* expression is restored to
726 pre-treatment endogenous levels (siRNA 0.5nM), confirming the antiproliferative effect of CRIM1.
727 n=6 with eight technical replicates for each condition. **(C).** Western Blot analysis shows ERK
728 phosphorylation (pERK) at 24 hours after UVA treatment in HCE-S cells. The increased ERK
729 phosphorylation due to UVA exposure was brought back to normal levels following transfection
730 with 0.5nM CRIM1 siRNA. **(D).** *BCL2* expression, measured by qRT-PCR, decreases upon UVA

731 irradiation eliciting apoptosis but is restored in HCE-S cells treated with siCRIM1. Data represent $2^{-\Delta\Delta Ct}$ ± SEM with respect to untransfected HCE-S. n=3 with three technical replicates each sample.

733

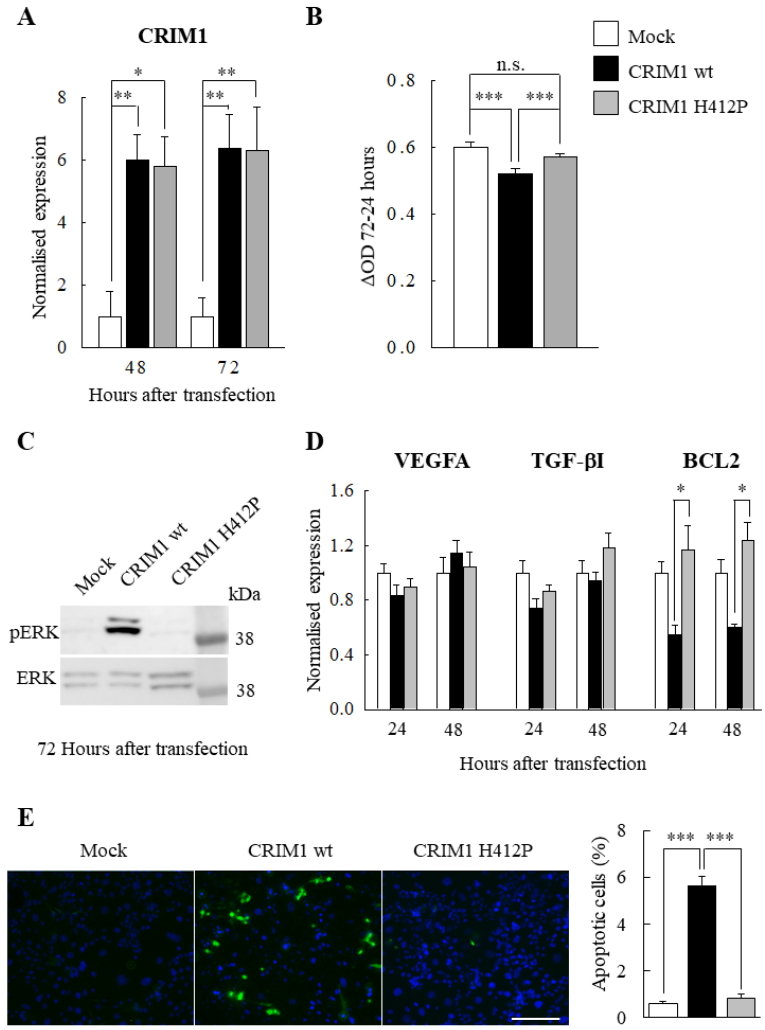

734

735 **Figure 6.** *CRIM1* wild type overexpression in HCE-S cells results in a decrease in cell proliferation
736 and an increase in ERK phosphorylation and apoptosis. **(A).** qRT-PCR showing *CRIM1*
737 overexpression in mRNA obtained from HCE-S cells transfected with Human *CRIM1* wild type and
738 mutant (H412P) in pcDNA3.1 expression plasmid. Both *CRIM1* wild type (wt) and H412P mutant
739 were significantly overexpressed at 48 and 72 hours after transfection with respect to the mock
740 control. Data represent fold change of the $2^{-\Delta Ct}$ mean ± SEM. n=3 with 3 technical replicates for each
741 condition. **(B).** An MTT assay of HCE-S cell proliferation was performed at 72 hours after
742 transfection with empty plasmid (mock), *CRIM1* wt and H412P mutant constructs. *CRIM1* wt, when
743 overexpressed, has an anti-proliferative effect when compared to the mock transfected control
744 ($p<0.001$). Overexpression of the mutated H412P *CRIM1* does not have the same anti-proliferative

effect. n=6 with 8 technical replicates for each condition. **(C).** ERK phosphorylation (pERK) was detected by Western Blot analysis at 72 hours post transfection with mock, *CRIM1* wt and H412P plasmids in HCE-S cells. *CRIM1* wt overexpression resulted in a high level of ERK phosphorylation in comparison to *CRIM1* H412P and mock control. **(D).** qRT-PCR analysis of *VEGFA*, *TGF-βI* and *BCL2* expression in HCE-S cells transfected with mock, CRIM1 wt and H412P plasmids and harvested after 48 and 72 hours. No significant variation of *VEGFA* and *TGF-βI* expression was observed between mock, *CRIM1* wt and *CRIM1* H412P while *BCL2* expression significantly decreased in H412 wt CRIM1 transfected cells compared with mock transfected HCE-S both at 48 and 72 hours post transfection. Data represent fold change of the $2^{-\Delta Ct}$ mean ± SEM respect to mock transfected HCE-S. n=3 with three technical replicates each. **(E).** TUNEL assay in HCE-S cells transfected with wt and H412P mutant *CRIM1* plasmids. TUNEL-positive cells are stained green and nuclei are stained blue with DAPI. Overexpression of CRIM1 wt results in increased apoptosis compared to either the *CRIM1* H412P or mock transfected cells. Scale bar, 100 μm. TUNEL assay quantification was performed in 12 fields per condition using ImageJ. n=3

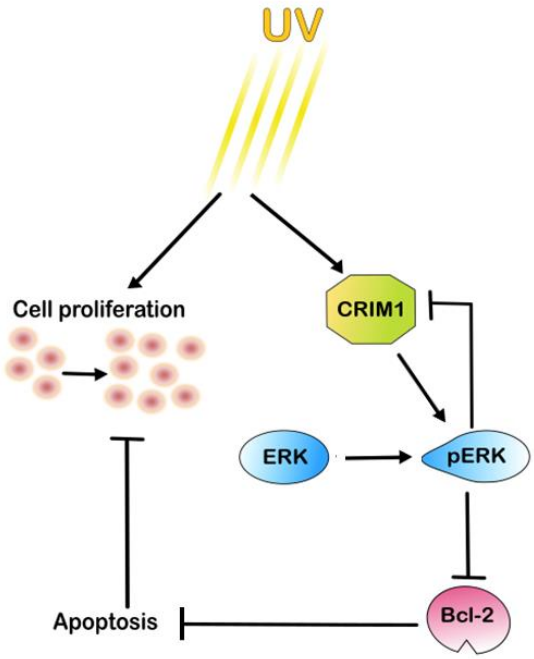

Figure 7. CRIM1 regulates pERK in a looped pathway. Here, based on our experimental evidence, we propose, within a schematic, an intracellular pathway triggered by UV that may act as a protective mechanism against pterygium development. When cells are exposed to UV light, CRIM1 expression is increased, which in turn increases ERK phosphorylation. This, in turn, blocks further CRIM1 expression in the feedback loop shown. Inhibition of ERK phosphorylation prevents this negative feedback, resulting in further increases of CRIM1 expression.

ERK phosphorylation induces decreased expression of the anti-apoptotic BCL2, initiating cell apoptosis. This proposed pathway was shown to be impaired in the case of the H412P mutation in CRIM1, found in the Northern Irish family affected by pterygium.

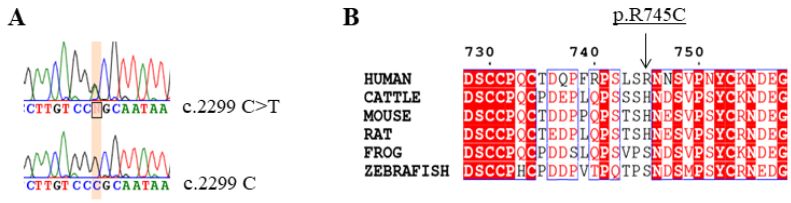

775

776 **Supplementary Figure 1.** R745C variant found in a pterygium affected patient from Bolivia. **(A).**
777 Electropherogram showing the novel c.2299C>T transition variant from the Bolivian patient (B1),
778 which corresponds to the R745C variant**. (B).** Multiple *CRIM1* sequence alignment shows that the
779 R745 residue is not conserved across species; it is conserved however the absence of cysteine between
780 VWFC-4 (residues 677-735) and VWFC-5 (residues 751-809).

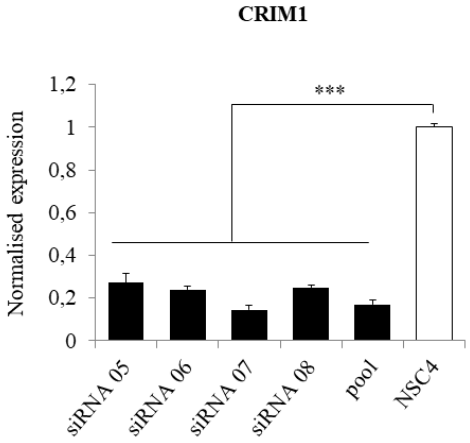

781

782 **Supplementary Figure 2.** siRNAs targeting *CRIM1* efficiently knock down its expression in HCE-
783 S cells. *CRIM1* expression obtained using qRT-PCR of HCE-S cell cDNA 48 hours post transfection.
784 All four siRNAs tested were able to knock down *CRIM1* expression, including the pool of four
785 siRNAs used at the same final concentration of 10 nM. qRT-PCR data represent fold change of the
786 $2^{-\Delta\Delta Ct}$ mean ± SEM with respect to untreated HCE-S. n=2 with three technical replicates each.

787

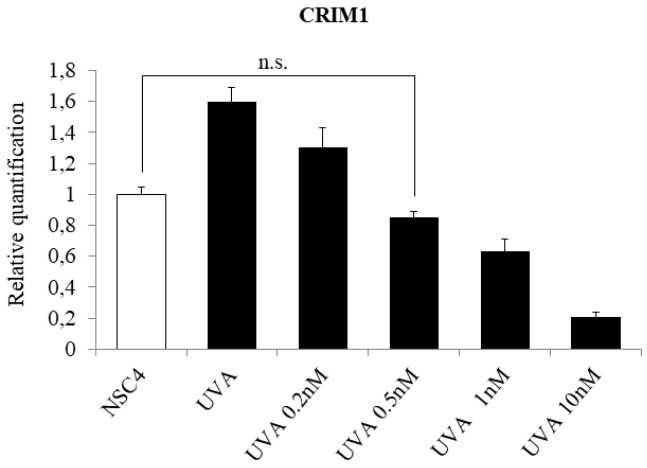

788

789 **Supplementary Figure 3.** A dose response curve shows that 0.5nM siRNA pool restores HCE-S
790 endogenous *CRIM1* levels. *CRIM1* expression obtained using qRT-PCR of HCE-S cell cDNA 48
791 hours post transfection with UVA and the siRNA pool at different concentrations. qRT-PCR data
792 represent fold change of the $2^{-\Delta\Delta Ct}$ mean ± SEM with respect to untreated HCE-S. n=2 with three
793 technical replicates each.

794

TABLES

Family member	Year of birth	Sex	Eye condition	Age of diagnosis	Lived abroad	Time in sunny climates	Wear sunglasses
II.2	1944	F	pterygium	40 years	No	1/year, 3 weeks	Sometimes
II.4	1946	F	pterygium	59 years	Canada 13 years	1/year, 2 weeks	No
II.9	1958	M	unaffected	-	No	1/year, 3 weeks	Yes
II.14	1951	M	pterygium	62 years	No	1/year, 1 week	Yes
III.2	1967	M	unaffected	-	No	1/year, 1 week	Yes
III.3	1982	F	unaffected	-	No	1/year, 1 week	Sometimes
III.5	1968	F	pinguecula	38 years	Canada 13 years	1/year, 2 weeks	Sometimes
III.6	1970	F	pinguecula	40 years	Canada 13 years	1/year, 2 weeks	Sometimes

Table 1. Questionnaire results. The Northern Irish family members participating in the study are listed with age of pterygium diagnosis, averaged 48 years old. The family were shown not to have had excessive exposure to the sun, spending time in sunny climates from 1 to 3 weeks per years with most stating that they wear sunglasses.

Gene Symbol	Chr	Position	Gene Region	Protein Variant	Conservation to:	Gene expressed in:	Associated Diseases
CTRC	1	15764869	Promoter		Human	pancreas, liver, spleen	chronic pancreatitis
KIF21B	1	200978030	Exonic	p.T105M	Elephant	eye (cornea), brain, blood	multiple sclerosis, inflammatory bowel disease
GALNT14	2	31348076	Intronic; Exonic; 5'UTR	p.A58V	Human	kidney, PNS, blood, eye	breast cancer
CRIM1	2	36706700	Exonic	p.H412P	Lamprey	placenta, kidney, PNS, eye	syndactyly, neuronitis, bovine ocular carcinoma
SPTBN1	2	54886366	Exonic	p.T2107A; p.T2094A	Dog	tongue, soft tissue, eye	fissured tongue, and buphthalmos
VRK2	2	58313555	Exonic; ncRNA	p.G113E; p.G90E	Elephant	lymph node, testis, colon	vaccinia, and hypoxia
PLEK	2	68615546	Exonic	p.N229H	X_tropicalis	bone marrow, lymph node, eye	aarskog-scott syndrome, centronuclear myopathy
HNMT	2	138772049	3'UTR		Dog	bladder, kidney, liver, eye	asthma, eosinophilia-myalgia syndrome
ITGB6	2	160994200	Exonic	p.H469N	Mouse	pancreas, tongue, stomach, eye	bullous keratopathy, mouth disease
WDR12	2	203760891	Exonic	p.L169S	Zebrafish	blood, intestine, thymus, eye	gigantism, and neuronal ceroid lipofuscinosis
CLDN16	3	190106072	Exonic	p.A56fs*16	Rhesus	kidney, ovary, uterus	nephrocalcinosis, and hypomagnesemia primary
CLDN16	3	190106074	Exonic	p.A56P	Rhesus	kidney, ovary, uterus	nephrocalcinosis, and hypomagnesemia primary
PRIM2	6	57398226	Exonic	p.G310V	Human	thymus, ovary, mammary, eye	
STK31	7	23811795	Exonic; ncRNA	p.N598_S600delinsKKI	Elephant	testis	
TYW1	7	66660242	Exonic	p.H632R	Human	stomach, heart, colon, eye	fanconi's anemia, and cytochrome p450
GLDC	9	6556206	Exonic	p.I717V	Zebrafish	small intestine, kidney, liver, eye	glycine encephalopathy
IFNA5	9	21304891	Exonic	p.C122S	Elephant	_____	hemorrhagic fever
DMRTA1	9	22451120	Exonic	p.K242R	Rhesus	_____	metabolic acidosis, prostatitis
MIR4289	9	91360776	microRNA		Dog	_____	
HBG2	11	5276282	Promoter		Rhesus	spleen, thymus, liver	sulfhemoglobinemia, cavernous hemangioma
OR4C16	11	55339462	Promoter		Human	_____	neuronitis
OR10AG1	11	55735808	Exonic	p.H43D	Rhesus	_____	neuronitis
C12orf56	12	64712620	Exonic; Intronic	p.T210I	Human	_____	
ATP8B4	15	50223420	Exonic; ncRNA	p.R513Q	Lamprey	blood, bone marrow	intrahepatic cholestasis
DMXL2	15	51773329	Exonic	p.D1356N; p.D1992N	Chicken	blood, testis, heart, eye	gynecomastia, and myocardial infarction
TPSD1	16	1306802	Exonic	p.I87V	Human	_____	asthma, allergic and inflammatory disorders
TPSD1	16	1306817	Exonic	p.A92T	Human	_____	asthma, allergic and inflammatory disorders
NOMO1	16	18544469	Exonic	p.R418H	Chicken	intestine, cervix, colon, eye	pseudoxanthoma elasticum (PXE)
SRCAP	16	30731568	Exonic	p.R968H	Chicken	Larynx, thymus, spleen, eye (cornea)	floating-harbor syndrome, Eosinophilic angiocentric fibrosis
ZNF319	16	58031913	Exonic	p.A86V	Elephant	bladder, blood, tongue	
PDPR	16	70154480	Exonic	p.T29A	Human	heart, bone, Eye	sarcosinemia
ZFHX3	16	72832474	Exonic	p.454_455insH; p.1368_1369insH	X_tropicalis	_____	prostate cancer, acute myocardial infarction
WWOX	16	78466409	Exonic	p.L272F	Rhesus	mammary, tongue, PNS, eye	toxic pneumonitis, andaspiration pneumonitis
GSDMA	17	38122680	Exonic	p.V128L	Human	_____	atopy, gastric cancer
DNAI2	17	72306188	Intronic; Exonic	p.V460V	Elephant	testis, uterus, lung, brain	ciliary dyskinesia
MAN2B1	19	12774537	Exonic	p.P248L	Dog	bone, PNS, intestine, eye	alpha-mannosidosis, alpha-mannosidosis, adult form
CYP4F2	19	15989730	Exonic	p.T472A	Mouse	intestine, blood, liver, muscle	warfarin sensitivity, cytochrome p450
PRKD2	19	47204207	Exonic	p.V167M; p.V324M	Lamprey	Spleen, tongue, ovary, eye	polycystic kidney disease, gastric cancer
NLRP7	19	55451405	Exonic	p.P261Q	X_tropicalis	_____	gestational trophoblastic neoplasm, hydatidiform mole
TTC3	21	38569884	Exonic	p.G1865S	X_tropicalis	Tongue, uterus, heart, eye	down syndrome critical region, down syndrome

802

Gene Symbol	Translation Impact	SIFT Function Prediction	SIFT Score	PolyPhen-2 Function Prediction	dbSNP ID	NHLBI ESP European Frequency (%)	Co-segregation within the family (IGV)					
							II.2	II.4	III.5	III.6	II.14	II.9
CTRC					144717165		Het	Het	Hom WT	Het	Het	Hom WT
KIF21B	missense	Damaging	0,01	Benign	150551633	0,01	Het	Het	Het	Het	Het	Hom WT
GALNT14	missense	Tolerated	0,26	Benign	41280621		Het	Het	Het	Het	Het	Hom WT
CRIM1	missense	Damaging	0,01	Probably Damaging	113372122	0,29	Het	Het	Het	Het	Het	Hom WT
SPTBN1	missense	Tolerated	0,72	Benign	147989241	0,16	Het	Het	Het	Hom WT	Het	Hom WT
VRK2	missense	Damaging	0,02	Benign	147530902	0,36	Het	Het	Het	Hom WT	Het	Hom WT
PLEK	missense	Tolerated	0,52	Benign	34338164	1,14	Het	Het	Het	Hom WT	Het	Hom WT
HNMT							Het	Het	Het	Hom WT	Het	Hom WT
ITGB6	missense	Tolerated	0,65	Benign	142197545	0,29	Het	Het	Hom WT	Het	Het	Hom WT
WDR12	missense	Damaging	0	Possibly Damaging		0	Het	Het	Hom WT	Het	Het	Hom WT
CLDN16	frameshift				56086318	0	Het	Het	Het	Het	Het	Hom WT
CLDN16	missense	Damaging	0,04	Benign	3214506	0	Het	Het	Het	Het	Het	Hom WT
PRIM2	missense				77436138		Het	Het	Het	Het	Het	Hom WT
STK31	in-frame					0	Het	Het	Het	Het	Het	Hom WT
TYW1	in-frame	Tolerated	0,5	Benign		0	Het	Het	Het	Het	Het	Hom WT
GLDC	missense	Tolerated	1	Benign	117460214	0,03	Het	Het	Hom WT	Het	Het	Hom WT
IFNA5	missense	Damaging	0	Probably Damaging	140371188	0,59	Het	Het	Hom WT	Hom WT	Het	Hom WT
DMRTA1	missense	Tolerated	0,54	Benign	145718826	0,38	Het	Het	Hom WT	Hom WT	Het	Hom WT
MIR4289							Het	Het	Het	Hom WT	Het	Hom WT
HBG2					113622787		Het	Het	Het	Hom WT	Het	Hom WT
OR4C16							Het	Het	Hom m	Het	Het	Hom WT
OR10AG1	in-frame	Activating	1	Benign		0	Het	Het	Hom m	Het	Het	Hom WT
C12orf56	missense	Tolerated	0,13		367932023	0,03	Het	Het	Hom WT	Het	Het	Hom WT
ATP8B4	missense	Damaging	0	Probably Damaging		0	Het	Het	Hom WT	Het	Het	Hom WT
DMXL2	missense	Tolerated	0,17	Benign	144241909	0,02	Het	Het	Hom WT	Het	Het	Hom WT
TPSD1	missense	Tolerated	0,31	Benign	2401930	0	Het	Het	Het	Het	Het	0
TPSD1	missense	Tolerated	0,75	Benign	3993983	0	Het	Het	Het	Het	Het	0
NOMO1	missense	Tolerated	0,23	Benign	140359200	0,12	Het	Het	Hom WT	Hom WT	Het	Hom WT
SRCAP	missense	Damaging	0	Possibly Damaging	368876335	0,01	Het	Het	Hom WT	Het	Het	Hom WT
ZNF319	missense	Tolerated	0,08	Benign		0	Het	Het	Hom WT	Het	Het	0
PDPR	missense	Tolerated	1	Benign	200469748	0	Het	Het	Het	Het	Het	Het
ZFHX3	in-frame					0	Het	Het	Hom WT	Het	Het	Hom WT
WWOX	missense	Tolerated	0,7	Benign	186745328	0,46	Het	Het	Hom WT	Het	Het	Hom WT
GSDMA	missense	Activating	1	Benign		0	Het	Het	Het	Het	Het	Hom WT
DNAI2	synonymous				148947094	0,05	Het	Het	Hom WT	Het	Het	Hom WT
MAN2B1	missense	Damaging	0,01	Possibly Damaging	117843968	0,42	Het	Het	Het	Het	Het	Hom WT
CYP4F2	missense	Tolerated	0,39	Benign	4020346	0	Het	Het	Hom WT	Hom WT	Het	Hom WT
PRKD2	missense	Tolerated	0,15	Benign	45455991	0,98	Het	Het	Hom WT	Het	Het	Hom WT
NLRP7	missense	Damaging	0	Probably Damaging		0	Het	Het	Het	Hom WT	Het	Hom WT
TTC3	missense	Tolerated	0,55	Possibly Damaging		0	Het	Het	Het	Hom WT	Het	Hom WT

803

Table 2. Candidate genes analysis. The table shows the 40 genes obtained from Ingenuity and the analysis done for each of the associated variants. The selection was mainly based on the expression of the gene in the eye (TIGER database), the SIFT and Polyphen predictions and known diseases association (literature review). Subsequently the aminoacid conservation through vertebrate species (BLAST analysis) and co-segregation of the mutation in pterygium (II.2, II.4, II.14) and pinguecula (III.5, III.6) affected members and not in the II.9 unaffected family member (IGV analysis) was considered. This screening led to the selection of *CRIM1* as the best candidate considering those parameters.

A.

Patient NI	Year of birth	Sex	Eye condition
1	1942	M	pterygium
2	1950	M	minor pterygium
3	1931	M	pterygium
4	1954	M	pterygium
5	1946	M	pterygium
6	1975	M	pterygium
7	1941	M	pterygium
8	1958	F	pterygium
9	1984	F	pterygium
10	1934	M	pterygium
11	1974	F	pterygium
12*	1967	F	pterygium family

B.

Patient Bolivia	Year of birth	Sex	Eye condition
B1	1965	F	pterygium
B2		M	pterygium
B3	1949	M	pterygium
B4	1957	M	pterygium
B5	1999	M	pterygium
B6	1952	M	pterygium
B7	1947	F	pterygium
B8	1941	M	pterygium
B9	1990	M	pterygium

Table 3. Individual pterygium participants. **(A).** A list of pterygium affected individuals collected in the UK and the relevant information obtained through the questionnaire. *Patient 12 denotes the pterygium affected II.1 family member previously studied[27]. **(B).** List of pterygium affected individuals collected in Bolivia and the year of birth and sex of participants.

CRIM1 sequence	Primer sequence (5’ to 3’)
T7_F	TAATACGACTCACTATAGGG
Seq1_R	GCAGAATGTGCAGTCGTCTT
Seq1_F	TGATCGAGGGTTATGCTCCT
Seq2_F	TACTACGTGCCCGAAGGAGA
Seq2_R	GGCACTTTCACAGGGTTTGT
Seq3_F	TGCCGGGAATGCTACTGT
Seq3_R	ACAGAAGGGCAGGACTCAGA
Seq4_F	CTGAGTCCTGGAAGCCTGAC
Seq4_R	CCTGGAGGTGACCCATATCT
Seq5_F	AACCATCGAGGAGAGGTTGA
Seq5_R	TCGTCTTCCGTCTTTTGAAAC

Supplementary Table 1. Primers used to validate that the whole of the CRIM1 sequence was inserted into the pcDNA3.1 plasmid and to check the presence of the H412P mutation introduced by site directed mutagenesis.

CRIM1 VWFs	Primer sequence (5' to 3')
Exon6_F (VWF1)	TTGAAAAACATCAAAGGACACAA
Exon6_R (VWF1)	CCATGTATGCTCCTGTTAATCTG
Exon7_F (VWF2)	GATGACTAGAACCCAGGGAAAA
Exon7_R (VWF2)	AGCAGACATTATGCCCAAGG
Exon11_F (VWF3)	GCCTGTTTCTCCTGTGCAGT
Exon11_R (VWF3)	TGCAAGGCAGAAGTCATTTG
Exon12_F (VWF4)	CCAGGCTTTCAAGAGTTGGA
Exon12_R (VWF4)	GGGTCCCACAGAATGACAAC
Exon13_F (VWF5)	CTGGCCAACAGCATCTTCTT
Exon13_R (VWF5)	GACATGTCAAGCAGGGAAAAA
Exon14_F (VWF6)	AAGATCGTGTGCGTTGTCAC
Exon14_R (VWF6)	GTCGAGCTCTGCTTCGATTT

Supplementary Table 2. Primers used to verify the presence of other mutations in all the VWF domains of CRIM1.

8. REFERENCES

1 Chui, J., Di Girolamo, N., Wakefield, D. & Coroneo, M. T. The pathogenesis of pterygium: current concepts and their therapeutic implications. *The ocular surface* **6**, 24-43 (2008).

2 Das, P. *et al.* Limbal epithelial stem-microenvironmental alteration leads to pterygium development. *Molecular and cellular biochemistry* **402**, 123-139, doi:10.1007/s11010-014-2320-z (2015).

3 Bianchi, E. *et al.* Immunohistochemical profile of VEGF, TGF-beta and PGE(2) in human pterygium and normal conjunctiva: experimental study and review of the literature. *Int J Immunopathol Pharmacol* **25**, 607-615 (2012).

4 Detorakis, E. T. & Spandidos, D. A. Pathogenetic mechanisms and treatment options for ophthalmic pterygium: trends and perspectives (Review). *International journal of molecular medicine* **23**, 439 (2009).

5 Ono, T. *et al.* Long-term follow-up of transplantation of preserved limbal allograft and amniotic membrane for recurrent pterygium. *Graefe's Archive for Clinical and Experimental Ophthalmology*, 1-6 (2016).

6 Kaji, Y. *et al.* Immunohistochemical localization of advanced glycation end products in pinguecula. *Graefe's archive for clinical and experimental ophthalmology = Albrecht von Graefes Archiv fur klinische und experimentelle Ophthalmologie* **244**, 104-108, doi:10.1007/s00417-005-0047-y (2006).

7 Jakobiec, F. A., Rashid, A., Bozorg, M. S. & Dana, R. Unusual large uniocular elastoid and collagenous pinguecula. *Graefe's archive for clinical and experimental ophthalmology = Albrecht von Graefes Archiv fur klinische und experimentelle Ophthalmologie* **252**, 1173-1175, doi:10.1007/s00417-014-2649-8 (2014).

8 Lemercier, G., Cornand, G. & Burckhart, M. F. [Pinguecula and pterygium: histologic and electron microscopic study (author's transl)]. *Virchows Archiv. A, Pathological anatomy and histology* **379**, 321-333 (1978).

9 Moran, D. J. & Hollows, F. C. Pterygium and ultraviolet radiation: a positive correlation. *British Journal of Ophthalmology* **68**, 343-346 (1984).

10 Taylor, H. R. *et al.* Corneal changes associated with chronic UV irradiation. *Archives of Ophthalmology* **107**, 1481-1484 (1989).

11 McCarty, C. A., Fu, C. L. & Taylor, H. R. Epidemiology of pterygium in Victoria, Australia. *British Journal of Ophthalmology* **84**, 289-292 (2000).

12 Zhong, H. *et al.* Ethnic Variations in Pterygium in a Rural Population in Southwestern China: The Yunnan Minority Eye Studies. *Ophthalmic Epidemiol* **23**, 116-121, doi:10.3109/09286586.2015.1099685 (2016).

13 Gazzard, G. *et al.* Pterygium in Indonesia: prevalence, severity and risk factors. *British journal of ophthalmology* **86**, 1341-1346 (2002).

14 Lombardo, M., Pucci, G., Barberi, R. & Lombardo, G. Interaction of ultraviolet light with the cornea: clinical implications for corneal crosslinking. *Journal of cataract and refractive surgery* **41**, 446-459, doi:10.1016/j.jcrs.2014.12.013 (2015).

15 Coroneo, M., Müller-Stolzenburg, N. & Ho, A. Peripheral light focusing by the anterior eye and the ophthalmohelioses. *Ophthalmic Surgery, Lasers and Imaging Retina* **22**, 705-711 (1991).

16 Kau, H. C., Tsai, C. C., Hsu, W. M., Liu, J. H. & Wei, Y. H. Genetic polymorphism of hOGG1 and risk of pterygium in Chinese. *Eye (Lond)* **18**, 635-639, doi:10.1038/sj.eye.6700738 (2004).

17 Tsai, Y. Y. *et al.* Null type of glutathione S-transferase M1 polymorphism is associated with early onset pterygium. *Mol Vis* **10**, 458-461 (2004).

18 Di Girolamo, N., Wakefield, D. & Coroneo, M. T. UVB-mediated induction of cytokines and growth factors in pterygium epithelial cells involves cell surface receptors and

intracellular signaling. *Invest Ophthalmol Vis Sci* **47**, 2430-2437, doi:10.1167/iovs.05-1130 (2006).
19 Di Girolamo, N., Coroneo, M. T. & Wakefield, D. UVB-elicited induction of MMP-1 expression in human ocular surface epithelial cells is mediated through the ERK1/2 MAPK-dependent pathway. *Investigative ophthalmology & visual science* **44**, 4705-4714 (2003).
20 Chao, S. C. *et al.* Ultraviolet-A irradiation upregulated urokinase-type plasminogen activator in pterygium fibroblasts through ERK and JNK pathways. *Invest Ophthalmol Vis Sci* **54**, 999-1007, doi:10.1167/iovs.12-10469 (2013).
21 Coroneo, M. T. Pterygium as an early indicator of ultraviolet insolation: a hypothesis. *The British journal of ophthalmology* **77**, 734-739 (1993).
22 Gallagher, M. J., Giannoudis, A., Herrington, C. S. & Hiscott, P. Human papillomavirus in pterygium. *The British journal of ophthalmology* **85**, 782-784 (2001).
23 Piras, F. *et al.* Detection of human papillomavirus DNA in pterygia from different geographical regions. *The British journal of ophthalmology* **87**, 864-866 (2003).
24 BOOTH, F. Heredity in one hundred patients admitted for excision of pterygia. *Australian and New Zealand journal of ophthalmology* **13**, 59-61 (1985).
25 Ang, M. *et al.* Prevalence of and racial differences in pterygium: a multiethnic population study in Asians. *Ophthalmology* **119**, 1509-1515 (2012).
26 Zhang, J. D. An investigation of aetiology and heredity of pterygium. Report of 11 cases in a family. *Acta Ophthalmol (Copenh)* **65**, 413-416 (1987).
27 Romano, V., Steger, B., Kovacova, A., Kaye, S. B. & Willoughby, C. E. Further evidence for heredity of pterygium. *Ophthalmic genetics*, 1-3, doi:10.3109/13816810.2015.1111911 (2016).
28 Hecht, F. & Shoptaugh, M. G. Winglets of the eye: dominant transmission of early adult pterygium of the conjunctiva. *J Med Genet* **27**, 392-394 (1990).
29 Contrucci Faraldi, N. & Gracis, G. Pterygium on twins. *Ophthalmologica* **172**, 361-366 (1976).
30 Hill, J. C. & Maske, R. Pathogenesis of pterygium. *Eye (Lond)* **3 (Pt 2)**, 218-226, doi:10.1038/eye.1989.31 (1989).
31 Islam, S. I. & Wagoner, M. D. Pterygium in young members of one family. *Cornea* **20**, 708-710 (2001).
32 Tsai, Y.-Y. *et al.* Null type of glutathione S-transferase M1 polymorphism is associated with early onset pterygium. *Molecular vision* **10**, 458-461 (2004).
33 Tsai, Y. Y. *et al.* Pterygium and genetic polymorphism of DNA double strand break repair gene Ku70. *Mol Vis* **13**, 1436-1440 (2007).
34 Demurtas, P. *et al.* Association between the ACE insertion/deletion polymorphism and pterygium in Sardinian patients: a population based case-control study. *BMJ open* **4**, e005627, doi:10.1136/bmjopen-2014-005627 (2014).
35 Chen, P.-L. *et al.* XRCC1, but not APE1 and hOGG1 gene polymorphisms is a risk factor for pterygium. (2010).
36 Taylor, J. C. *et al.* Factors influencing success of clinical genome sequencing across a broad spectrum of disorders. **47**, 717-726, doi:10.1038/ng.3304 (2015).
37 Nesbit, M. A. *et al.* Mutations in AP2S1 cause familial hypocalciuric hypercalcemia type 3. *Nature genetics* **45**, 93-97 (2013).
38 Robert, X. & Gouet, P. Deciphering key features in protein structures with the new ENDscript server. *Nucleic acids research* **42**, W320-W324 (2014).
39 Untergasser, A. *et al.* Primer3—new capabilities and interfaces. *Nucleic acids research* **40**, e115-e115 (2012).
40 Moore, J. E. *et al.* Effect of tear hyperosmolarity and signs of clinical ocular surface pathology upon conjunctival goblet cell function in the human ocular surface. *Investigative ophthalmology & visual science* **52**, 6174-6180, doi:10.1167/iovs.10-7022 (2011).

945 41 Nesbitt, H. *et al.* Nitric Oxide Up-Regulates RUNX2 in LNCaP Prostate Tumours:
946 Implications for Tumour Growth In Vitro and In Vivo. *Journal of cellular physiology* **231**,
947 473-482 (2016).
948 42 Schmittgen, T. D. & Livak, K. J. Analyzing real-time PCR data by the comparative CT
949 method. *Nature protocols* **3**, 1101-1108 (2008).
950 43 Kulkarni, B., Mohammed, I., Hopkinson, A. & Dua, H. S. Validation of endogenous control
951 genes for gene expression studies on human ocular surface epithelium. *PloS one* **6**, e22301,
952 doi:10.1371/journal.pone.0022301 (2011).
953 44 Notara, M. & Daniels, J. T. Characterisation and functional features of a spontaneously
954 immortalised human corneal epithelial cell line with progenitor-like characteristics. *Brain*
955 *Res Bull* **81**, 279-286, doi:10.1016/j.brainresbull.2009.08.009 (2010).
956 45 Wilkinson, L. *et al.* CRIM1 regulates the rate of processing and delivery of bone
957 morphogenetic proteins to the cell surface. *J Biol Chem* **278**, 34181-34188,
958 doi:10.1074/jbc.M301247200 (2003).
959 46 Vinals, F. & Pouyssegur, J. Confluence of vascular endothelial cells induces cell cycle exit
960 by inhibiting p42/p44 mitogen-activated protein kinase activity. *Molecular and cellular*
961 *biology* **19**, 2763-2772 (1999).
962 47 Kaya, A. I. *et al.* Cell contact-dependent functional selectivity of beta2-adrenergic receptor
963 ligands in stimulating cAMP accumulation and extracellular signal-regulated kinase
964 phosphorylation. *The Journal of biological chemistry* **287**, 6362-6374,
965 doi:10.1074/jbc.M111.301820 (2012).
966 48 Moore, J. E. *et al.* Protection of corneal epithelial stem cells prevents ultraviolet A damage
967 during corneal collagen cross-linking treatment for keratoconus. *The British journal of*
968 *ophthalmology* **98**, 270-274, doi:10.1136/bjophthalmol-2013-303816 (2014).
969 49 Allen, E. H. *et al.* Allele-Specific siRNA Silencing for the Common Keratin 12 Founder
970 Mutation in Meesmann Epithelial Corneal DystrophyAllele-Specific siRNA Silencing.
971 *Investigative ophthalmology & visual science* **54**, 494-502 (2013).
972 50 Lovicu, F., Kolle, G., Yamada, T., Little, M. & McAvoy, J. Expression of Crim1 during
973 murine ocular development. *Mechanisms of development* **94**, 261-265 (2000).
974 51 Pennisi, D. J. *et al.* Crim1KST264/KST264 mice display a disruption of the Crim1 gene
975 resulting in perinatal lethality with defects in multiple organ systems. *Developmental*
976 *Dynamics* **236**, 502-511 (2007).
977 52 Beleggia, F. *et al.* CRIM1 haploinsufficiency causes defects in eye development in human
978 and mouse. *Hum Mol Genet* **24**, 2267-2273, doi:10.1093/hmg/ddu744 (2015).
979 53 Hocking, J. C. *et al.* Morphogenetic defects underlie Superior Coloboma, a newly identified
980 closure disorder of the dorsal eye. **14**, e1007246, doi:10.1371/journal.pgen.1007246 (2018).
981 54 Nakashima, Y. *et al.* Inhibition of the proliferation and acceleration of migration of vascular
982 endothelial cells by increased cysteine-rich motor neuron 1. *Biochem Biophys Res Commun*
983 **462**, 215-220, doi:10.1016/j.bbrc.2015.04.118 (2015).
984 55 Eulalio, A. *et al.* Functional screening identifies miRNAs inducing cardiac regeneration.
985 *Nature* **492**, 376-381, doi:10.1038/nature11739 (2012).
986 56 Ferguson, S. W. *et al.* The microRNA regulatory landscape of MSC-derived exosomes: a
987 systems view. *Scientific reports* **8**, 1419 (2018).
988 57 Ponferrada, V. G. *et al.* CRIM1 complexes with ss-catenin and cadherins, stabilizes cell-cell
989 junctions and is critical for neural morphogenesis. *PloS one* **7**, e32635,
990 doi:10.1371/journal.pone.0032635 (2012).
991 58 Zhang, Y. *et al.* Crim1 regulates integrin signaling in murine lens development.
992 *Development*, doi:10.1242/dev.125591 (2015).
993 59 Zeng, H. *et al.* CRIM1, a newfound cancer-related player, regulates the adhesion and
994 migration of lung cancer cells. *Growth factors (Chur, Switzerland)* **33**, 384-392,
995 doi:10.3109/08977194.2015.1119132 (2015).

60 Fan, J. *et al.* Crim1 maintains retinal vascular stability during development by regulating endothelial cell Vegfa autocrine signaling. *Development* **141**, 448-459 (2014).
61 Glienke, J., Sturz, A., Menrad, A. & Thierauch, K. H. CRIM1 is involved in endothelial cell capillary formation in vitro and is expressed in blood vessels in vivo. *Mech Dev* **119**, 165-175 (2002).
62 Wilkinson, L. *et al.* Crim1KST264/KST264 mice implicate Crim1 in the regulation of vascular endothelial growth factor-A activity during glomerular vascular development. *J Am Soc Nephrol* **18**, 1697-1708, doi:10.1681/asn.2006091012 (2007).
63 Pausch, H. *et al.* Identification of QTL for UV-protective eye area pigmentation in cattle by progeny phenotyping and genome-wide association analysis. *PLoS One* **7**, e36346, doi:10.1371/journal.pone.0036346 (2012).
64 Gerber, T. *et al.* Mapping heterogeneity in patient-derived melanoma cultures by single-cell RNA-seq. *Oncotarget* (2016).
65 Kolle, G., Georgas, K., Holmes, G. P., Little, M. H. & Yamada, T. CRIM1, a novel gene encoding a cysteine-rich repeat protein, is developmentally regulated and implicated in vertebrate CNS development and organogenesis. *Mechanisms of development* **90**, 181-193 (2000).
66 O'Leary, J. M. *et al.* Solution structure and dynamics of a prototypical chordin-like cysteine-rich repeat (von Willebrand Factor type C module) from collagen IIA. *The Journal of biological chemistry* **279**, 53857-53866, doi:10.1074/jbc.M409225200 (2004).
67 Kinna, G. *et al.* Knockdown of zebrafish crim1 results in a bent tail phenotype with defects in somite and vascular development. *Mechanisms of development* **123**, 277-287 (2006).
68 Kria, L., Ohira, A. & Amemiya, T. Immunohistochemical localization of basic fibroblast growth factor, platelet derived growth factor, transforming growth factor-beta and tumor necrosis factor-alpha in the pterygium. *Acta Histochem* **98**, 195-201 (1996).
69 Wu, M. *et al.* Overexpression of low-density lipoprotein receptors stimulated by vascular endothelial growth factor in fibroblasts from pterygium. *Biomed Pharmacother* **93**, 609-615, doi:10.1016/j.biopha.2017.06.090 (2017).
70 Chui, J. *et al.* Ophthalmic pterygium: a stem cell disorder with premalignant features. *Am J Pathol* **178**, 817-827, doi:10.1016/j.ajpath.2010.10.037 (2011).
71 Dushku, N. & Reid, T. W. Immunohistochemical evidence that human pterygia originate from an invasion of vimentin-expressing altered limbal epithelial basal cells. *Curr Eye Res* **13**, 473-481 (1994).
72 Gebhardt, M. *et al.* Differential expression of vascular endothelial growth factor implies the limbal origin of pterygia. *Ophthalmology* **112**, 1023-1030, doi:10.1016/j.ophtha.2005.01.023 (2005).
73 Wilkinson, L. *et al.* Crim1KST264/KST264 mice implicate Crim1 in the regulation of vascular endothelial growth factor-A activity during glomerular vascular development. *Journal of the American Society of Nephrology* **18**, 1697-1708 (2007).
74 Marionnet, C., Tricaud, C. & Bernerd, F. Exposure to non-extreme solar UV daylight: spectral characterization, effects on skin and photoprotection. *International journal of molecular sciences* **16**, 68-90 (2014).
75 Courtney, D. G. *et al.* siRNA silencing of the mutant keratin 12 allele in corneal limbal epithelial cells grown from patients with Meesmann's epithelial corneal dystrophy. *Invest Ophthalmol Vis Sci* **55**, 3352-3360, doi:10.1167/iovs.13-12957 (2014).
76 Cagnol, S. & Chambard, J. C. ERK and cell death: mechanisms of ERK-induced cell death--apoptosis, autophagy and senescence. *The FEBS journal* **277**, 2-21, doi:10.1111/j.1742-4658.2009.07366.x (2010).
77 Liang, K. *et al.* Expression of cell proliferation and apoptosis biomarkers in pterygia and normal conjunctiva. (2011).

78 Kwok, L. S. & Coroneo, M. T. A model for pterygium formation. *Cornea* **13**, 219-224 (1994).
79 Nakashima, Y. & Takahashi, S. Induction of cysteine-rich motor neuron 1 mRNA expression in vascular endothelial cells. *Biochemical and biophysical research communications* **451**, 235-238, doi:10.1016/j.bbrc.2014.07.108 (2014).
80 Kannabiran, C. & Klintworth, G. K. TGFBI gene mutations in corneal dystrophies. *Human mutation* **27**, 615-625 (2006).
81 Tan, D. T., Tang, W. Y., Liu, Y. P., Goh, H. S. & Smith, D. R. Apoptosis and apoptosis related gene expression in normal conjunctiva and pterygium. *The British journal of ophthalmology* **84**, 212-216 (2000).
82 Mencucci, R. *et al.* Effects of riboflavin/UVA corneal cross-linking on keratocytes and collagen fibres in human cornea. *Clinical & experimental ophthalmology* **38**, 49-56 (2010).
83 Buron, N. *et al.* Differential mechanisms of conjunctival cell death induction by ultraviolet irradiation and benzalkonium chloride. *Investigative ophthalmology & visual science* **47**, 4221-4230 (2006).
84 Yam, J. C. & Kwok, A. K. Ultraviolet light and ocular diseases. *International ophthalmology* **34**, 383-400 (2014).
85 Cullen, A. P. Photokeratitis and other phototoxic effects on the cornea and conjunctiva. *International journal of toxicology* **21**, 455-464 (2002).
86 DILLON, J., Zheng, L., MERRIAM, J. C. & GAILLARD, E. R. The optical properties of the anterior segment of the eye: implications for cortical cataract. *Experimental eye research* **68**, 785-795 (1999).
87 Newton, R., Reeves, G., Beral, V., Ferlay, J. & Parkin, D. Effect of ambient solar ultraviolet radiation on incidence of squamous-cell carcinoma of the eye. *The Lancet* **347**, 1450-1451 (1996).
88 Lucas, R. M., McMichael, A. J., Armstrong, B. K. & Smith, W. T. Estimating the global disease burden due to ultraviolet radiation exposure. *International journal of epidemiology* **37**, 654-667 (2008).
89 Hirst, L. W. Distribution, risk factors, and epidemiology of pterygium. *Pterygium, Kugler Publications, The Hague, The Netherlands*, 15-27 (2000).
90 Raghunath, A. & Perumal, E. Micro-RNAs and their roles in eye disorders. *Ophthalmic research* **53**, 169-186, doi:10.1159/000371853 (2015).
91 Tam, O. H. *et al.* Crim1 is required for maintenance of the ocular lens epithelium. *Experimental eye research* **170**, 58-66, doi:10.1016/j.exer.2018.02.012 (2018).
92 Machens, A. *et al.* Age-related penetrance of endocrine tumours in multiple endocrine neoplasia type 1 (MEN1): a multicentre study of 258 gene carriers. *Clinical endocrinology* **67**, 613-622 (2007).
93 Vitt, U. A., Hsu, S. Y. & Hsueh, A. J. Evolution and classification of cystine knot-containing hormones and related extracellular signaling molecules. *Molecular endocrinology* **15**, 681-694 (2001).
94 Pearton, D. J., Ferraris, C. & Dhouailly, D. Transdifferentiation of corneal epithelium: evidence for a linkage between the segregation of epidermal stem cells and the induction of hair follicles during embryogenesis. *The International journal of developmental biology* **48**, 197-201, doi:10.1387/ijdb.031744dp (2004).
95 Engelsvold, D. H. *et al.* miRNA and mRNA expression profiling identifies members of the miR-200 family as potential regulators of epithelial-mesenchymal transition in pterygium. *Exp Eye Res* **115**, 189-198, doi:10.1016/j.exer.2013.07.003 (2013).
96 Watson, S. *et al.* Limbal dermoid epithelium shares phenotypic characteristics common to both hair epidermal and limbal epithelial stem cells. *Current eye research* **38**, 835-842, doi:10.3109/02713683.2013.780625 (2013).

97 He, Y.-Y., Council, S. E., Feng, L. & Chignell, C. F. UVA-induced cell cycle progression is mediated by a disintegrin and metalloprotease/epidermal growth factor receptor/AKT/Cyclin D1 pathways in keratinocytes. *Cancer research* **68**, 3752-3758 (2008).
98 Assefa, Z., Van Laethem, A., Garmyn, M. & Agostinis, P. Ultraviolet radiation-induced apoptosis in keratinocytes: on the role of cytosolic factors. *Biochimica et Biophysica Acta (BBA)-Reviews on Cancer* **1755**, 90-106 (2005).
99 Moan, J. 7 Visible Light and UV Radiation. *Radiation*, 69 (2001).
100 Tsai, Y. Y. *et al.* Oxidative DNA damage in pterygium. *Molecular vision* **11**, 71-75 (2005).
101 Mercola, M. *et al.* Dominant-negative mutants of a platelet-derived growth factor gene. *Genes & development* **4**, 2333-2341 (1990).
102 Millauer, B., Shawver, L. K., Plate, K. H., Risaui, W. & Ullrich, A. Glioblastoma growth inhibited in vivo by a dominant-negative Flk-1 mutant. *Nature* **367**, 576-579 (1994).
103 Casari, C. *et al.* The dominant-negative von Willebrand factor gene deletion p. P1127_C1948delinsR: molecular mechanism and modulation. *Blood* **116**, 5371-5376 (2010).
104 Castaman, G., Eikenboom, J. C., Missiaglia, E. & Rodeghiero, F. Autosomal dominant type 1 von Willebrand disease due to G3639T mutation (C1130F) in exon 26 of von Willebrand factor gene: description of five Italian families and evidence for a founder effect. *British journal of haematology* **108**, 876-879 (2000).